

Control of Slag Carryover from the BOF Vessel During Tapping: BOF Cold Model Studies



ASHOK KAMARAJ, G.K. MANDAL, and G.G. ROY

In a modern integrated steel plant, slag-free tapping during transfer of liquid steel from the BOF vessel to the ladle is prerequisite to produce ultraclean steel for high-end critical applications. The present investigation aims to examine the drain vortices during the liquid steel tapping process. The tapping experiments were conducted in a geometrical down-scaled Perspex BOF cold model, which was more akin to the industrial practice than the other geometries previously reported in the literature. The study highlights the influence of the complex BOF shape on drain vortices during the tapping process. It is observed that vorticity behavior during liquid steel tapping from the BOF vessel is different from the earlier observations reported for the teeming process. The parametric study of the tapping process and its analysis confirmed that the threshold height for drain vortices is strongly influenced by the nozzle diameter (ND) and marginally influenced by the residual inertia of the liquid. The carryover ratio (COR) for the water-oil experiments is in agreement with the values obtained in industrial practice. Yield loss tends to increase with the increase in ND. The onset of drain vortices in the presence of overlying phase (oil/slag) during the BOF tapping process could be principally controlled by the vessel design. The physical properties of the overlying phase had negligible influence on the drain vortices. The critical times for vortex and drain sink formation were predicted based on dimensional analysis coupled with the mathematical formulation for the tapping process. A strategy to control the slag carryover during the tapping process in industry is also discussed and postulated based on the understanding developed from water modeling experiments.

<https://doi.org/10.1007/s11663-018-1432-3>

© The Minerals, Metals & Materials Society and ASM International 2018

I. INTRODUCTION

MODERN steelmaking operations can be divided broadly into three important stages, *i.e.*, refining, transfer operations, and solidification. One of the major challenges in transfer operation is proper monitoring of process parameters to restrict the carryover slag in transfer ladles. In industry practice, it is difficult to discard the overlying slag completely during transfer of liquid steel from one vessel to another (during tapping and teeming), as overlying slag always tends to carry-over along with the liquid steel.^[1–3] The slag entrapment during final stages of liquid steel processing (*i.e.*, teeming operation) adversely affects the quality of the

cast steel product. Therefore, slag entrapment during the teeming operation needs to be completely avoided to improve the cleanliness of cast steel. Research^[3–7] has been conducted for several decades to understand the slag carryover mechanisms and their control during liquid steel teeming from the ladle. Vortex formation at the critical liquid height (LH) and drain sink formation during the final stages of teeming are reported as the prime mechanisms for slag entrainment into liquid steel. It is reported that in the cold model simulation,^[3] oil (low-temperature analogue for slag) flow through the ladle nozzles breaks and entrains into the liquid steel as fine droplets and becomes entrapped during casting. Researchers^[3,5,8–11] have analyzed the conditions for the onset of vortex funnels during the teeming process using cold model simulation and dimensionless numbers. It was found that the major factors responsible for vortex formation during draining are residual motion in liquids from previous operation (tangential or rotational velocity), ladle and nozzle dimensions, dwell time (DT) of liquid steel in the ladle, nozzle eccentricity, *etc.*^[3,12] It is also reported that the density of overlying phase and the critical outflow rate influence the formation of nonvortex funnels such as drain sink.^[8] Based on the laboratory investigation results, Sankaranarayanan

ASHOK KAMARAJ and G.K. MANDAL are with the Academy of Scientific and Innovative Research (AcSIR), CSIR–National Metallurgical Laboratory (CSIR-NML), Jamshedpur 831 007, India. Contact emails: srhsbioboy@yahoo.co.in, ashokk@nmlindia.org G.G. ROY is with the Academy of Scientific and Innovative Research (AcSIR), CSIR–National Metallurgical Laboratory (CSIR-NML) and also with the Indian Institute of Technology, Kharagpur 721 302, India.

Manuscript submitted May 18, 2018.

Article published online October 22, 2018.

and Guthrie^[3] designed a vortex buster to arrest vortex funnels and demonstrated the same using water model experiments and industrial trials. Mazumdar *et al.*^[6] reported that vortex formation during tundish emptying limits the complete transfer of liquid steel into the mold and causes yield loss. In their study, it was identified that deployment of new flow modifiers with the slight change in tundish design significantly reduced the tundish yield loss. Kojola *et al.*^[8] studied the influence of ladle bottom geometry on drain sink formation and yield loss during industrial teeming practice. Singh^[10] investigated the effect of Reynolds and Froude numbers on the teeming process and identified that gravitational force and Froude number have more influence on the draining process. Apart from experimental investigations, many studies^[12,16–20] were solely based on numerical simulation to obtain more insight about the onset of vortex and drain sink formation. Li *et al.*^[12] pointed out that the Coriolis force and physical properties of steel have little effect on vortex formation compared to the nozzle dimensions and eccentricity. Davila *et al.*^[6] mentioned that the inclined ladle bottom favors vortex formation rather than preventing it. Marcela *et al.*^[20] modeled the steel-slag interfacial perturbations in the ladle teeming operation and optimized the parameters for maximum yield. Most of these investigations were carried out to understand the mechanisms and onset of slag carryover during teeming rather than quantification. The quantification for carryover slag is insignificant for teeming operations, as even little entrapment will deteriorate the quality of cast products.

The entrainment of slag during the tapping operation leads to metal cleanliness problems. The quality of the liquid steel during secondary refining stages depends on the composition and amount of carryover slag during the tapping operation. The presence of carryover (oxidizing) slag in the ladle after tapping acts as the source of impurities (such as phosphorus and oxygen in steel)^[21–23] and adversely affects desulfurization, recovery of alloying elements, and inclusion removal during the refining process.^[21,24–28] The influence of viscosity on the discharge of two-layer liquids through an orifice was studied by Liow *et al.*^[29] for industrial practice. Various slag detection systems, such as infrared (IR) camera, sensors, and continuous thermal mapping, are used for identification and control of the vortex during the liquid steel transfer process.^[30–36] Devices, such as DART, tap hole slide gate assisted slag stopper, and tap hole plugs, are also proposed to arrest slag carryover.^[34] In spite of several approaches for controlling slag during liquid steel tapping, techniques, such as DART and IR-based camera, are commercially used in the steel industries. However, the success in preventing slag to carry over into the ladle during tapping is inherently associated with intelligent placement of DART above the tap hole and limitation in the IR-based techniques in predicting the onset of slag carryover during the initial period. In addition to this, IR-based techniques are expensive and both technologies demand highly skilled operators to make the timely decision toward the end of the tapping process.

Available literature information pertaining to the onset of the vortex and drain sink during tapping of the BOF/LD vessel for various process conditions is still limited.^[36] Draining from a complex shape BOF vessel needs to be understood thoroughly under dynamic process conditions. It is also essential to explore the possible vessel/tap hole design changes for better control on slag carryover during the tapping process. To the best of the authors' knowledge, hardly any literature exists on optimizing the operating parameters of the BOF tapping process to arrest the carryover slag without much loss in the iron yield. Therefore, this investigation deals with the water model experiment of the tapping process under various process conditions in a geometrical down-scaled Perspex semi-BOF model more akin to the industrial practice than any other earlier reported geometries. The aim of this investigation is to establish correlations for the prediction of the onset of critical height for the vortex, drain sink, and yield loss in a 1/7 scale down BOF cold model using dimensional analysis. Another prime focus of this investigation is on developing a better approach to restrict the slag carryover from the BOF vessel during the tapping process. With this as an objective, a strategy to control the slag carryover during the tapping process in industry is discussed and postulated based on the understanding developed from the water modeling experiments.

II. EXPERIMENTAL PROCEDURE

For the water modeling study, a scale down (1/7) semi-BOF Perspex model was designed and fabricated. The main aim for fabricating the cold model was to independently study the influence of various process parameters on the slag carryover mechanism during the tapping process. The top, side, and rear views of the semi-BOF vessel along with the dimensions are schematically shown in Figures 1(a) through (d). The detailed design of the semi-BOF vessel reveals a cylindrical barrel portion with a gradually tapering annular cone and a tap hole. A schematic representation of the entire experimental setup is shown in Figure 2(a). Pictorial representation of the fabricated Perspex BOF model for the tapping study is shown in Figures 2(b) through (d). The complete assembled semi-BOF Perspex model for the tapping study consists of the semi-BOF vessel, collecting vessel, hydraulic jack, tap hole, and weighing machine (Figure 2(b)). The side view of the fabricated BOF model is shown in Figure 2(c). Figure 2(d) shows the arrangement of an underwater camera to monitor the vortex and drain sink events.

At the start of the experiment, the Perspex BOF vessel was filled with water up to different initial LHs (8, 11, and 14 cm) through a pipe fitted above the rear end of the vessel pointing vertically downward. One of the main aims of the study was to examine the effect of the initial LH and nozzle diameter (ND) on the drain vortices. Apart from the LH and ND, the initial filling flow rate (FR) and DT of the fluid after filling until tapping start are also considered in this investigation, to account for the residual motion in the liquids before

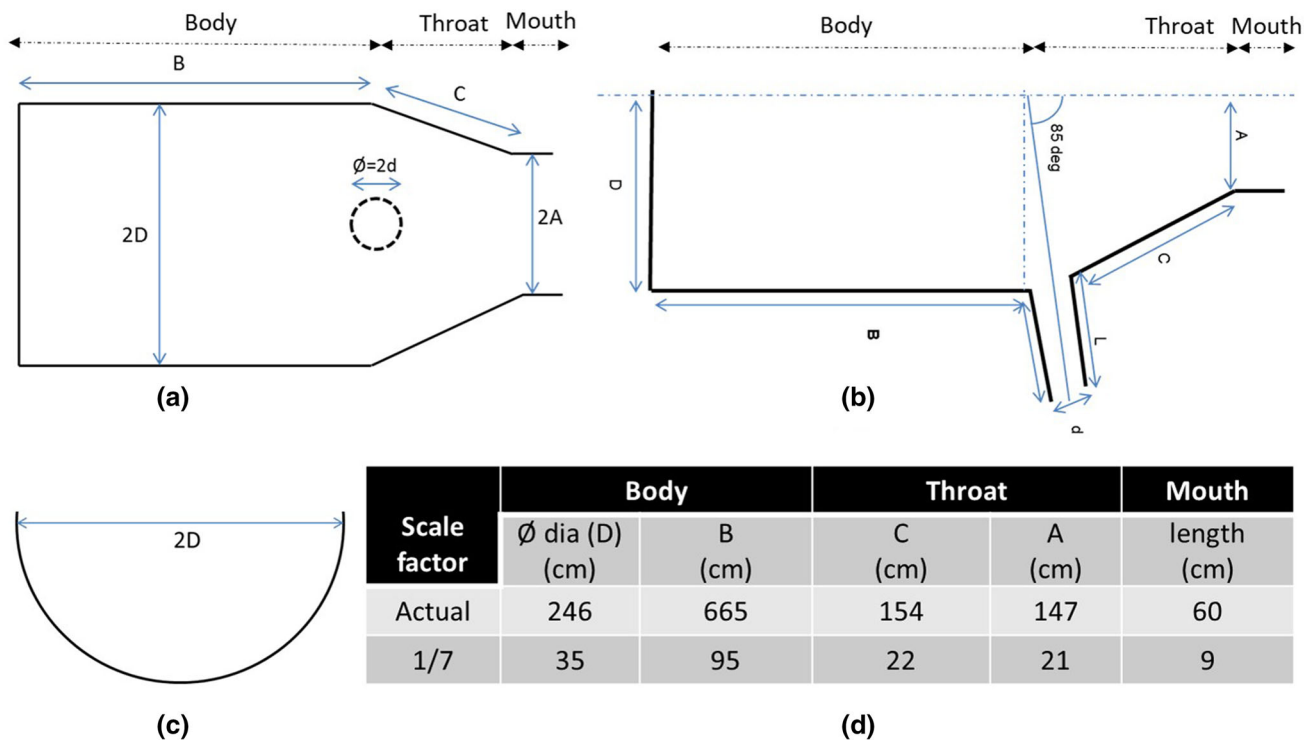


Fig. 1—Design details of the semi-BOF vessel: (a) top view, (b) side view, (c) rear view, and (d) dimension of various section of BOF vessel.

opening the nozzle.^[1–3] In the BOF steelmaking practice, some residual motion in the liquid is expected during the post blow period before tapping. The effect of such residual motion in liquid was taken care of by considering the FR and DT in the cold model simulation. The FR of water (20, 30, or 40 lpm) during filling was controlled and monitored using a digital contact flow meter. After filling, the water was allowed to remain at a standstill for a predefined DT (30, 60, or 90 seconds) prior to opening the tap hole for draining. A camera was placed on the back side of the transparent BOF vessel to monitor the progress of the LH as the draining time proceeded. An underwater camera (model: 1/16-in. VGA CMOS endoscope camera with 6 LED bright lights, frame rate: 30 FPS, focal distance: 3 to 10 cm, and waterproof capacity: IP67) with computer interface was also placed near the tap hole to record the occurrence of vortex and drain sink events. The formation of a dimple at the gas-liquid (water) interface was observed after a certain time of tapping. This dimple extended downward and formed a vortex tail with the increase in draining time. At the critical LH, where the vortex tail extends up to the tap hole, the overlying phase (air) may be entrained in the vortex and carried over to the transfer ladle. Toward the end of the tapping process, the vortex tail diminishes and converts into a drain sink for the overlying phase.^[17–19]

Therefore, tapping should be stopped at the onset of the drain sink to avoid the entrainment of overlying phase. During the tapping process, critical LH and time for vortex and drain sink formation were measured from the recorded image for all the experiments. The amount of water tapped out and retained in the BOF vessel was

measured carefully for analysis. The similar procedure was also adopted for water-oil experiments, where the known amount of oil is added into the BOF vessel, immediately after filling the vessel with water and prior to opening the tap hole. In the case of water-oil experiments, dimple forms at the oil/water interface and the vortex tail reaches the tap hole with the increase in draining time. The corresponding LH from the vessel bottom is measured as the critical LH for vortex formation. At the end of draining, the vortex head extends up to the air-oil interface and converts to drain sink for slag; the corresponding LH is noted as the critical LH for drain sink formation. The tap hole was immediately closed as soon as the appearance of oil in the collecting tub was noticed. After completion of the experiment, the weight of water tapped out from the BOF vessel was measured. Water and oil retained in the vessel were collected separately in the transparent measuring cylinders, and the liquids were allowed to settle for a prolonged time. After clear stratification in the liquid layers, the volume of the liquids was measured precisely directly from the scale on the measuring cylinder. Fresh oil was used for every water-oil experiment.

The detailed experimental plan adopted in this investigation is given in Table I. Experimental plan 1 mainly focused on establishing the discharge curves (or drain curves) for the identified process conditions. Experimental plan 2 includes 108 experiments to study the influence of various parameters, such as tap hole/ND, initial filling FR, initial LH, and DT, on the occurrence of the vortex as well as the drain sink in the BOF vessel during the tapping process. Average values of three

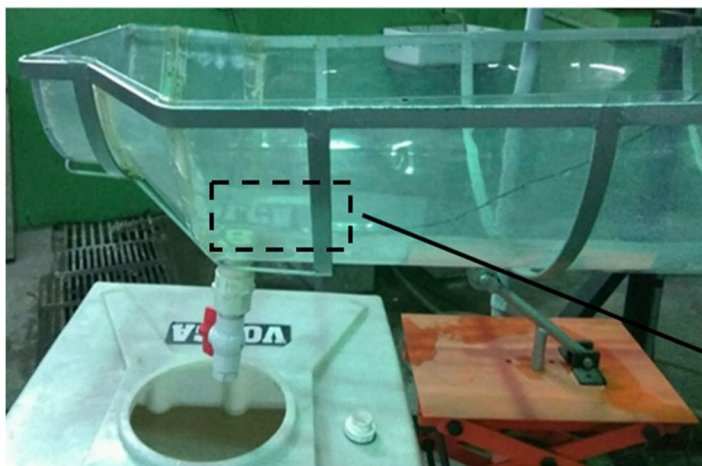
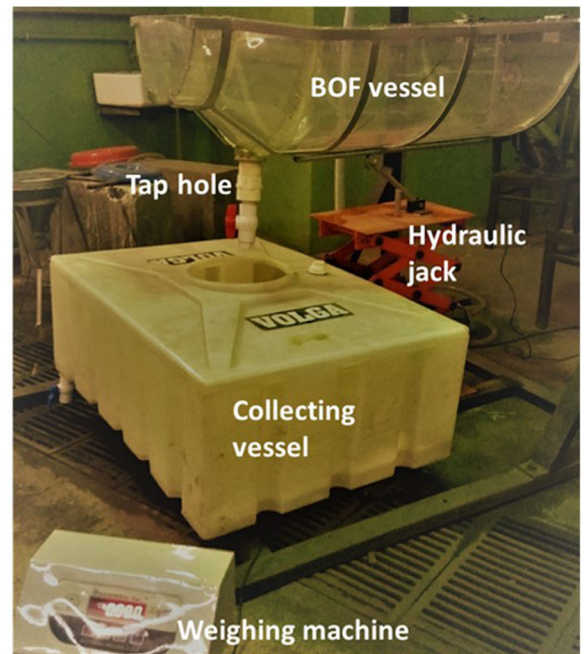
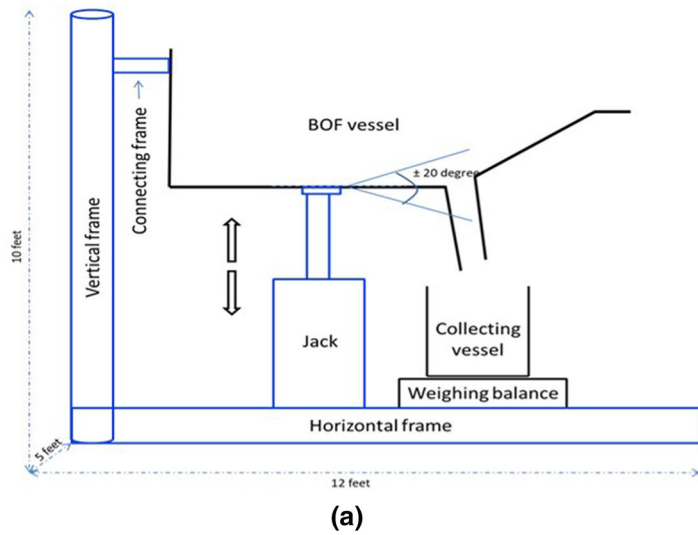


Fig. 2—(a) Schematic and (b) pictorial representation of the fabricated Perspex BOF model for tapping study, (c) side view of the fabricated BOF model, and (d) arrangement of an underwater camera to monitor the vortex and drain sink events.

trials were considered for vortex, drain sink, and yield loss analysis. In experimental plan 3, a set of experiments were carried out to study the influence of the various type of oils on vortex formation, yield loss, and overlying phase (oil) carryover during the tapping process. Another set of experiments (experimental plan 4) were also designed to study the influence of the amount of oil on yield loss and overlying phase carryover phenomena during the tapping process. The average values of two trials of water-oil experiments were taken for analysis.

III. RESULTS

A. Vortex and Drain Sink Observation

The underwater camera placed near the tap hole recorded the vortex and drain sink events occurring during the draining process. The pictorial representation of the vortex formation event during the tapping

experiment conducted in the BOF cold model is shown in Figure 3. The figure clearly demonstrates that the vortex begins with dimple formation (Figure 3(a)) in the free surface followed by extension of the tail toward the tap hole (Figures 3(b) through (d)) and establishes into the full vortex (Figure 3(e)) at the critical LH. Once the full vortex is established, the penetration of the air core to the flowing stream of water in the tap hole can be understood easily through the generation of a piercing sound. Toward the end of the tapping process, the extended vortex was converted to the drain sink, as shown in Figure 4 for all the studied NDs. The holelike appearance present in the upper portion of the figures is due to the reflection of light.

B. Drain Curve Analysis

The drain curve for the tapping experiments is described as the graph representing the decrease in the LH with respect to time proceeding toward emptying the BOF vessel. The influence of various process

Table I. Details of Experimental Plan

Solution Number	Plan	Parameters	Range	Number of Experiments
Drain curve analysis				
1	experimental plan 1	tap hole diameter	1.05 cm	16 experiments
2			1.44 cm	
3			1.77 cm	
4			2.14 cm	
5		filling FR	40 L/min	
6			20 L/min	
7		dwell/waiting time	30 s	
8			90 s	
9		initial LH	14 cm	
10			11 cm	
11			08 cm	
Effect of Parameters on Vortex and Drain Sink Formation				
12	experimental plan 2	tap hole diameter	1.05 cm	108 experiments repetition = 2 times average value of 3 trials were considered for analysis
13			1.44 cm	
14			1.77 cm	
15			2.14 cm	
16		filling FR	20 L/min	
17			30 L/min	
18			40 L/min	
19		dwell/waiting time	30 s	
20			60 s	
21			90 s	
22		initial LH	14 cm	
23	11 cm			
24	08 cm			
Effect of Different Oils on Vortex and Drain Sink Formation				
25	experimental plan 3	tap hole diameter	1.05 cm	12 experiments repetition = 1 time average value of 2 trials were considered for analysis
26			1.44 cm	
27			1.77 cm	
28			2.14 cm	
29		filling FR	20 L/min	
30		dwell/waiting time	90 s	
31		initial liquid (water) height	13 cm	
32		type of oils	coconut oil	
33			mustard oil	
34			petroleum ether	
35	oil height	1 cm		
Effect of Oil Height on Vortex and Drain Sink Formation				
36	experimental plan 4	tap hole diameter	1.44 cm	12 experiments repetition = 1 time average value of 2 trials were considered for analysis
37			2.14 cm	
38		filling FR	20 L/min	
39		dwell/waiting time	90 s	
40		initial liquid (water) height	13.5/13/12.5 cm	
41		type of oil	mustard oil	
42			coconut oil	
43		oil height	0.5 cm	
44			1 cm	
45		1.5 cm		

parameters on the typical drain curves for the tapping process is shown in Figure 5. Figures 5(a) and (b) represent the effect of variation of the ND on drain curves for the vessel filled with water up to the different initial LHs of 14, 11, and 8 cm at a constant flow rate of 40 lpm and DT of 60 seconds. Both figures clearly reveal that the drain curve significantly varies with the variation of both ND and initial LH. As expected, the decrease in the ND increases the total draining time for

a constant initial LH, whereas the total draining time increases with an increase in initial LH for a constant ND. Figure 5(c) depicts the effect of variation of DT on drain curves for the vessel filled with water up to an initial LH of 14 cm at a constant initial filling FR of 40 lpm and ND (FR) of 1.05 cm. Two different DTs of 30 and 90 seconds were used for comparison purposes. Figure 5(d) represents the drain curves for the vessel filled with water up to an initial LH of 14 cm at different

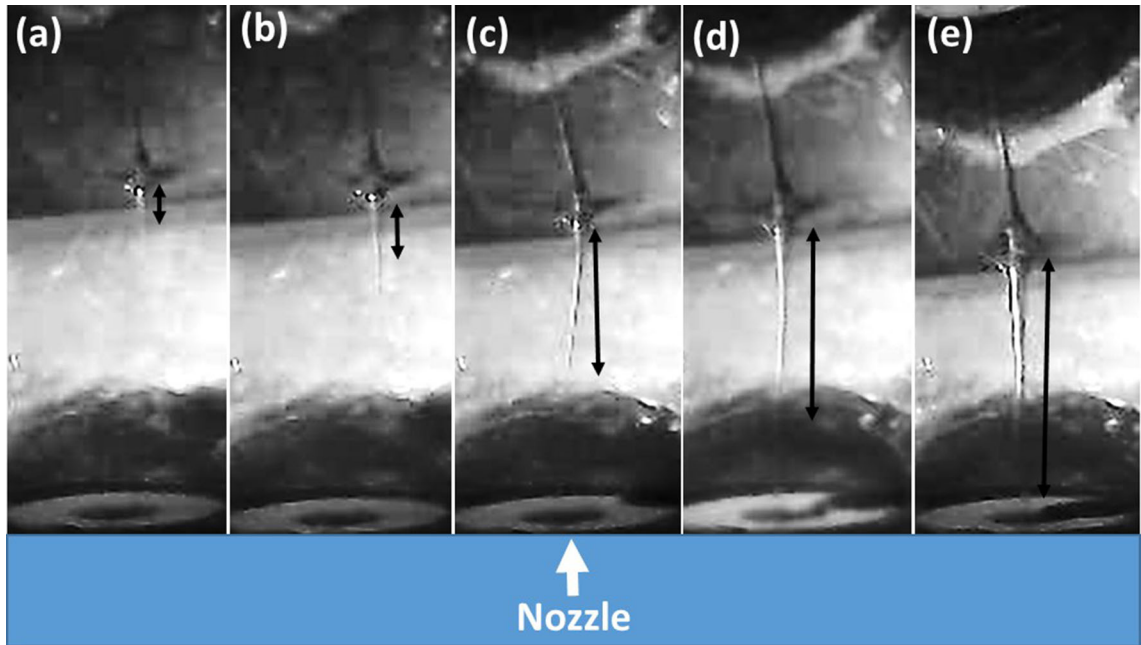


Fig. 3—Pictorial representation of the vortex formation event during the tapping experiment conducted in the BOF cold model: (a) dimple formation, (b) through (d) extension and tail formation, and (e) fully established vortex.

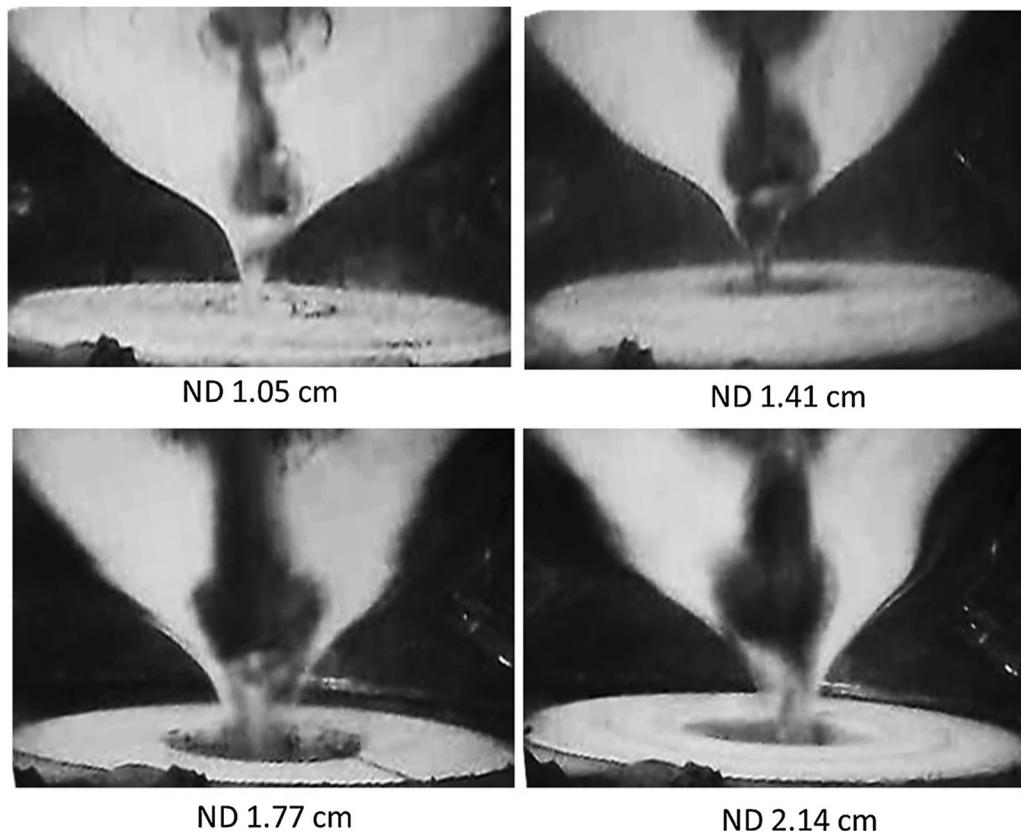


Fig. 4—Pictorial representation of the drain sink formation event during the tapping experiment conducted in the BOF cold model.

initial filling FRs of 20 and 40 lpm and constant DT of 60 seconds and ND of 1.05 cm. Figures 5(c) and (d) demonstrate that drain curves are identical and there is

no obvious variation in the progress of the drain curve with the variation of DT and FR, respectively. Therefore, the analysis of the drain curves suggests that both

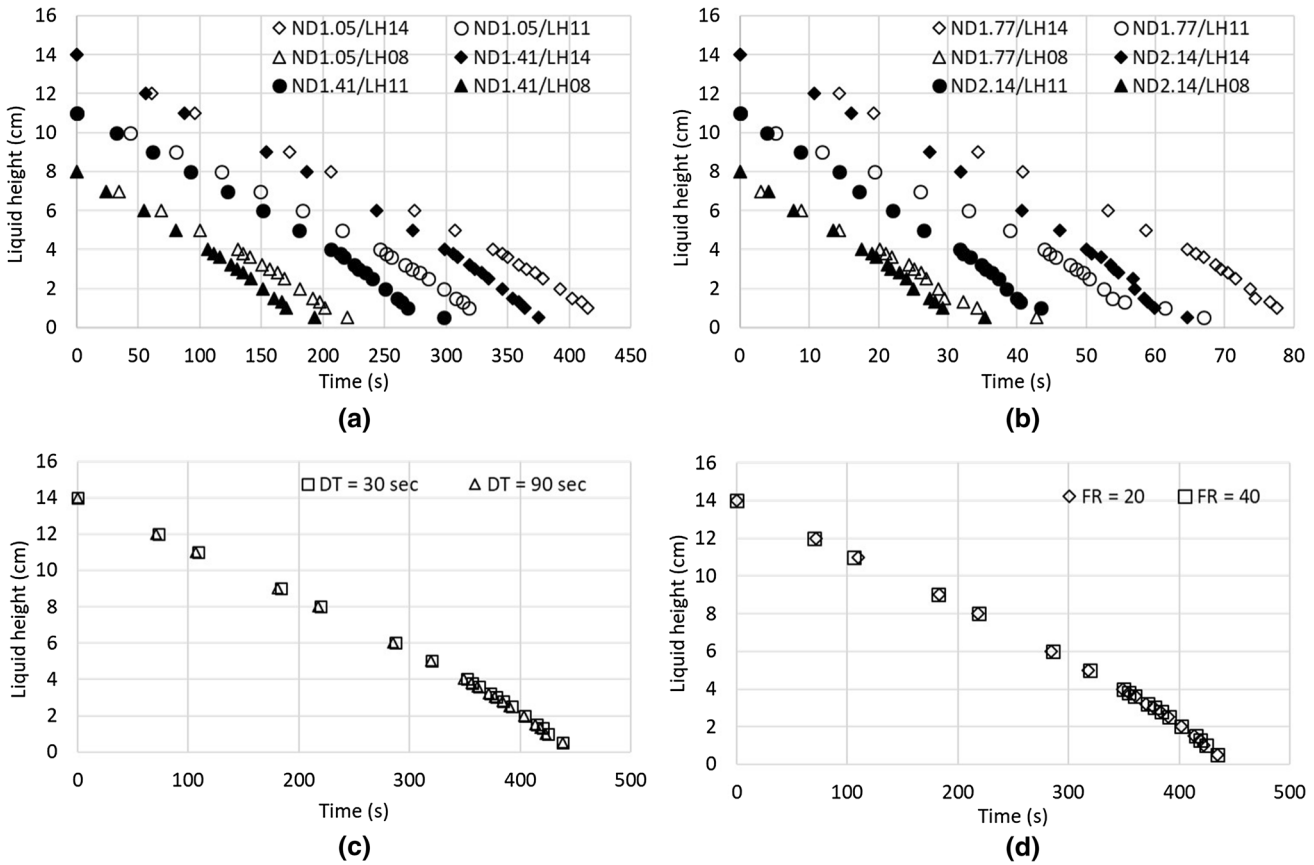


Fig. 5—Influence of (a) and (b) ND, (c) DT, and (d) initial filling FR on drain curves during the tapping process.

the FR and DT have a negligible influence on the trend of the drain curve in comparison with the ND and initial LH during the BOF tapping process.

C. Effect of Parameters on Critical Height for Vortex Formation

The effect of various parameters (*e.g.*, FR, DT, LH, and ND) on the critical LH for vortex formation (vortex height) is represented in Figure 6. Figures 6(a) through (d) represent the variation of the vortex height with the (a) DT for constant initial filling FR of 40 lpm, (b) initial LH for constant FR of 30 lpm, (c) FR for constant LH of 8 cm, and (d) ND for constant FR of 20 lpm. No significant variation of the vortex height with an increase in DT is observed for the experiments conducted with ND 1.05 and 1.41 cm (Figure 6(a)). However, a considerable increase in the vortex height is observed with an increase in the DT from 30 to 90 seconds for the experiments conducted with bigger ND, 1.77 and 2.14 cm. Figure 6(b) shows that the vortex height is less influenced by the initial LH for all the experiments conducted in the present study. It is evident from Figure 6(c) that the FR also shows similar behavior as that of the DT; *i.e.*, the influence of the FR on the vortex height is negligible for the experiments conducted with smaller NDs, while the FR influences the vortex height marginally for the bigger NDs of 1.77 and 2.14 cm. The variation of the vortex height as a

function of the ND is shown in Figure 6(d). Figure 6(d) demonstrates a significant increase in the vortex height with an increase in the ND from 1.05 to 2.14 cm.

Therefore, parametric analysis of the tapping process confirmed that the threshold height for vortex formation is strongly influenced by the ND. However, the marginal influence of the FR and DT on vortex formation only becomes significant at bigger NDs (1.77 and 2.14 cm). The average standard deviation for the data points of three trial experiments are given in the right side bottom corner of the figures as $\pm x$.

D. Effect of Parameters on Critical Height for Drain Sink Formation

Figure 7 shows the effect of various parameters (*e.g.*, FR, DT, LH, and ND) on the critical liquid height (LH) for drain sink (drain height) formation. It is observed that drain height is not significantly affected by the DT for the experiments conducted with different NDs for the constant FR of 20 lpm, as shown in Figure 7(a). It is also noted that the drain height is not influenced by the initial LH for all the experiments conducted with a constant FR of 40 lpm (Figure 7(b)). Variation of the drain height with the initial filling FR also does not show any significant effect (Figure 7(c)). It is also observed that the variation of the drain height gradually decreases as the FR increases from 30 to 40 lpm for bigger NDs (2.14 cm). Variation of the drain height with

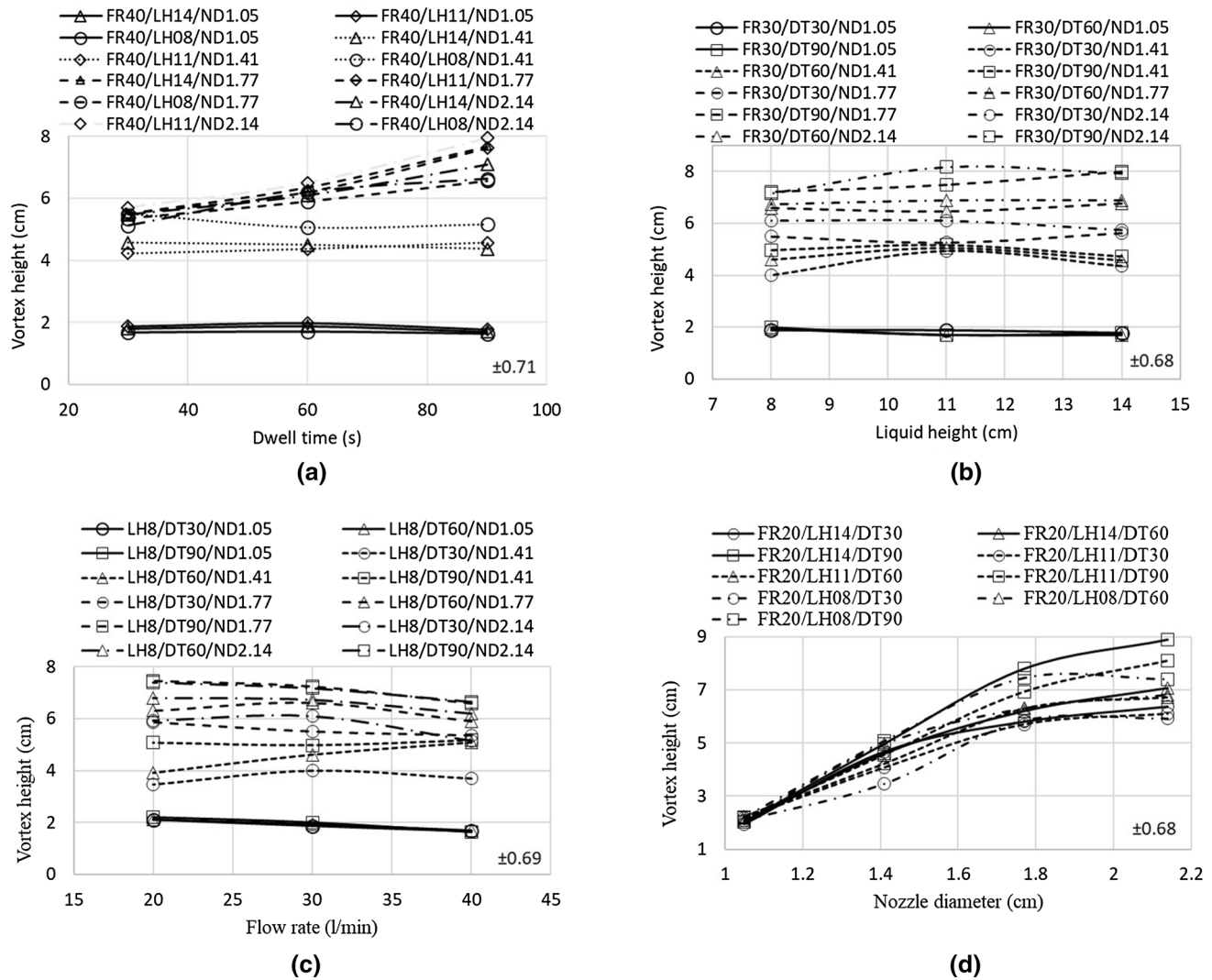


Fig. 6—Influence of (a) DT, (b) initial LH, (c) initial filling FR, and (d) ND on critical LH for vortex formation (vortex height). The numerical value on the right bottom corner of the figure represent the average standard deviation for all experimental data in the figure. Each experimental data represents the average value of three experimental trials.

different NDs for the experiments conducted with constant initial filling FR of 30 lpm is shown in Figure 7(d). A significant increase in the drain height with an increase in the ND from 1.05 to 2.14 cm can be observed from the figure. Therefore, it is concluded that the critical height for drain sink formation is strongly influenced by the ND and slightly influenced by the FR with bigger ND (2.14 cm).

E. Effect of Parameters on Yield Loss

Yield loss was estimated based on the amount of water left in the BOF vessel after the tapping process. The variation of the yield loss as a function of different process parameters is represented in Figure 8. Figure 8(a) depicts that the yield loss is not affected by the DT for the experiments conducted with different NDs at the constant initial FR of 30 lpm. Figure 8(b) shows that the yield loss is significantly influenced by the initial LH for all the experiments conducted with the

constant initial water filling FR of 20 lpm. Figure 8(c) depicts that the yield loss is not influenced by the FR. Figure 8(d) represents the variation of yield loss with different NDs, and a substantial increase in yield loss with the increase in ND is observed. Therefore, parametric analysis of the tapping process confirms that yield loss is strongly influenced by the ND and LH and not generally by the DT and FR.

F. Effect of Different Oils on the Tapping Process

In order to understand the effect of overlying phase (oil) on vortex and drain sink events during the tapping process, a set of water-oil experiments were also conducted with constant LHs (water: 13 cm and oil: 1 cm), constant FRs (20 lpm), and constant DTs (60 seconds) for different NDs. Experiments were performed with different types of oils including coconut oil, mustard oil, and petroleum ether. Variation of the critical height for vortex and drain sink formation with

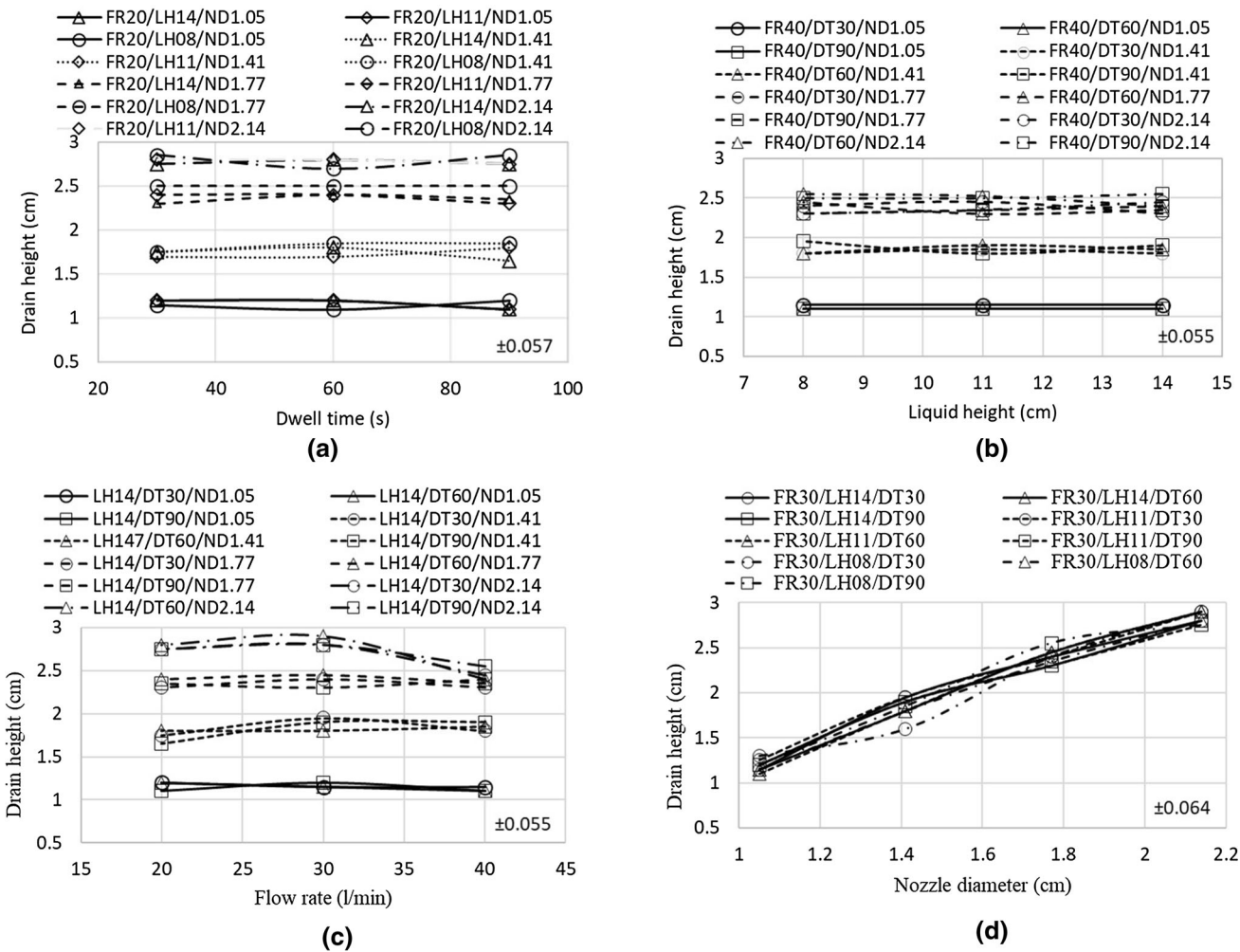


Fig. 7—Influence of (a) DT, (b) initial LH, (c) initial filling FR, and (d) ND on critical LH for drain sink formation (drain height). The numerical value on the right bottom corner of the figure represent the average standard deviation for all experimental data in the figure. Each experimental data represents the average value of three experimental trials.

variation of the ND in the presence of different overlying phases is represented in Figures 9(a) and (b), respectively. The figures show that the vortex and drain height increase with an increase in the ND for all the experiments conducted with and without oils. It is also observed that the critical height for vortex formation marginally decreases for the experiments conducted with oil (except ND 1.05 cm) in comparison to the experiments conducted without oil. However, the critical height for drain sink formation is greater for the experiments conducted with oils than those without oil. The variation of yield loss with different NDs for the constant FR of 20 lpm and DT of 90 seconds is shown in Figure 9(c). It was observed that the yield loss increases with the increase in ND from 1.05 to 2.14 cm when mustard oil and coconut oil are considered as overlying phases. However, an inconsistent trend was observed for the petroleum ether. The regular trend in the variation of yield loss for different types of oil for single ND was not observed. The oil (slag) carryover ratio (COR) is defined as the ratio of the amount of oil

carried over to the amount of water tapped during the tapping process. The variation of the COR with the different types of oils for the oil-water experiments using different NDs is shown in Figure 9(d). The COR is observed to be high for the experiments conducted with coconut oil as an overlying phase, except for the experiment conducted using an ND of 1.41 cm. In the case of ND 1.41 cm, the COR is maximum for the experiment conducted with petroleum ether as an overlying phase. Inconsistency in the yield loss and COR observed for the experiments conducted with petroleum ether as an overlying phase may be attributed to uncertainty in visual identification of oil carryover during tapping experiments because both petroleum ether and water are the same color.

In another set of water-oil experiments, the effect of thickness (amount) of oil phase on the tapping process was studied. The experiments were conducted with a fixed total initial liquid (oil + water) height of 14 cm with the variation of oil height (oil: 0.5, 1, and 1.5 cm) for the constant FR of 20 lpm and DT of 60 seconds.

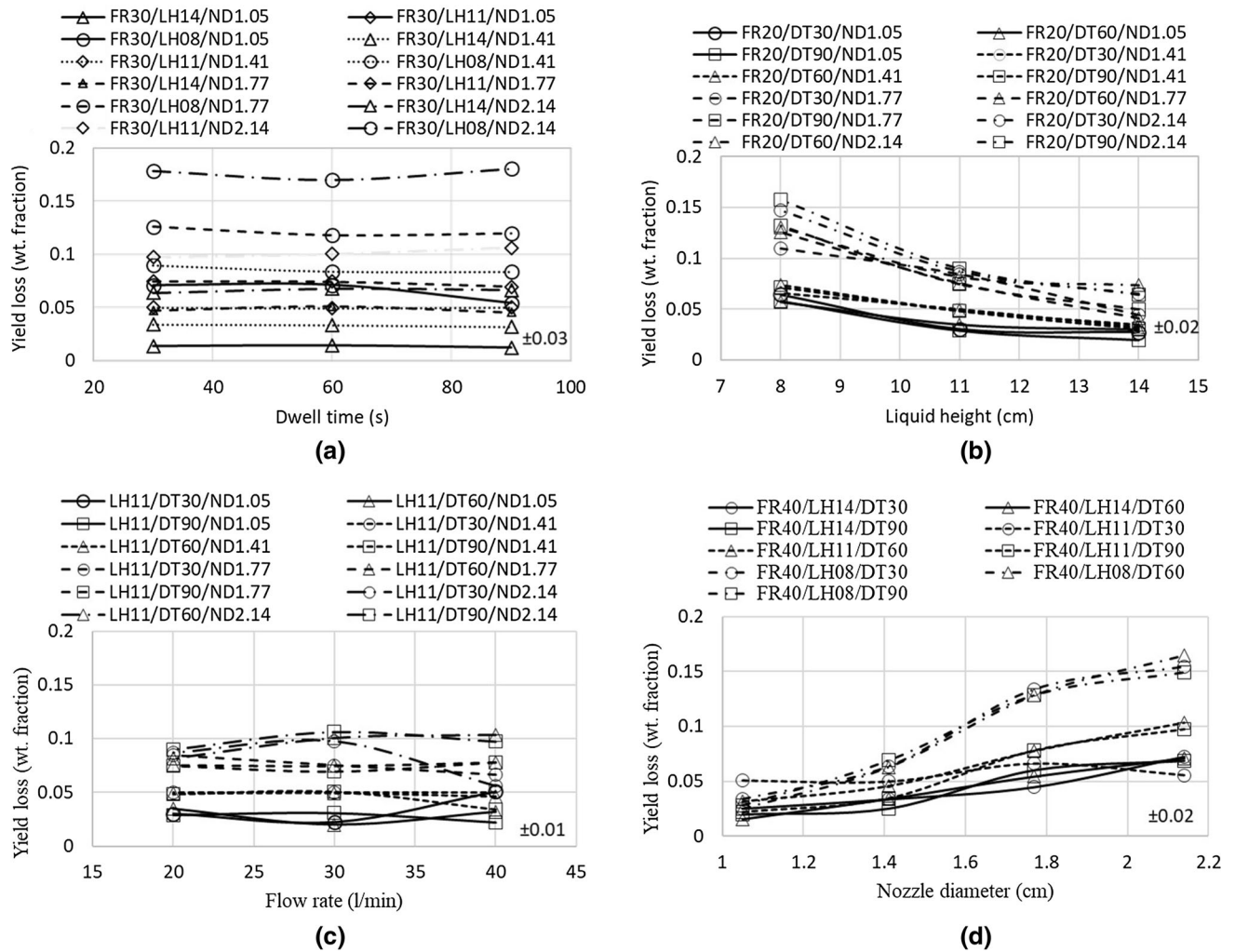


Fig. 8—Influence of (a) DT, (b) initial LH, (c) initial filling FR, and (d) ND on critical LH yield loss during the tapping process. The numerical value on the right bottom corner of the figure represent the average standard deviation for all experimental data in the figure. Each experimental data represents the average value of three experimental trials.

Due to the difficulty in conducting experiments with petroleum ether, this set of experiments were conducted with coconut oil and mustard oil as overlying phases for two different NDs of 1.41 and 2.14 cm. Variation of the vortex height with the amount of oils for different NDs is represented in Figure 10(a). The figure shows an increase in vortex height with an increase in oil layer thickness and ND.

Figure 10(b) depicts the increasing trend for drain height with the increase in initial oil height for both the NDs. Figure 10(c) reveals that yield loss is significantly high for the experiments conducted with ND of 2.14 cm for the different amounts of oil in comparison with ND 1.41 cm. It is also noticed that the lowest yield loss is observed for the experiments conducted with varying amounts of coconut oil for a single ND. The variation of the COR with oil thickness for two different oils as the overlying phase is shown in Figure 10(d). The COR generally increases with an increase in the amount of oil except for the experiment conducted with ND 2.14 cm and coconut oil as an overlying phase.

IV. DISCUSSION

A. Science Behind Vortex Formation in BOF Vessel

Several investigations^[10,12–15] reported in the literature provide understanding of the vortex dynamics in the ladle during the liquid steel teeming operation based on the results of the cold model and mathematical models. It is confirmed^[8,12] that initiation of the vortex during the draining process is mainly governed by the residual motion that exists in the liquids. It is inferred that the residual rotational motion that prevails in draining liquids accelerates to attain the vortex.^[14,15] In the case of higher ND, the rate of outflow is higher and the discharge rate is higher, which delays vortex formation (lowers the vortex height) in the ladle draining operation.^[14] Most of these studies were conducted using a vessel with a constant cross-sectional area, which is more likely to resemble the teeming process. In order to verify the existing knowledge for the BOF tapping process, a geometrical down-scaled semi-BOF cold model is fabricated to simulate the industrial

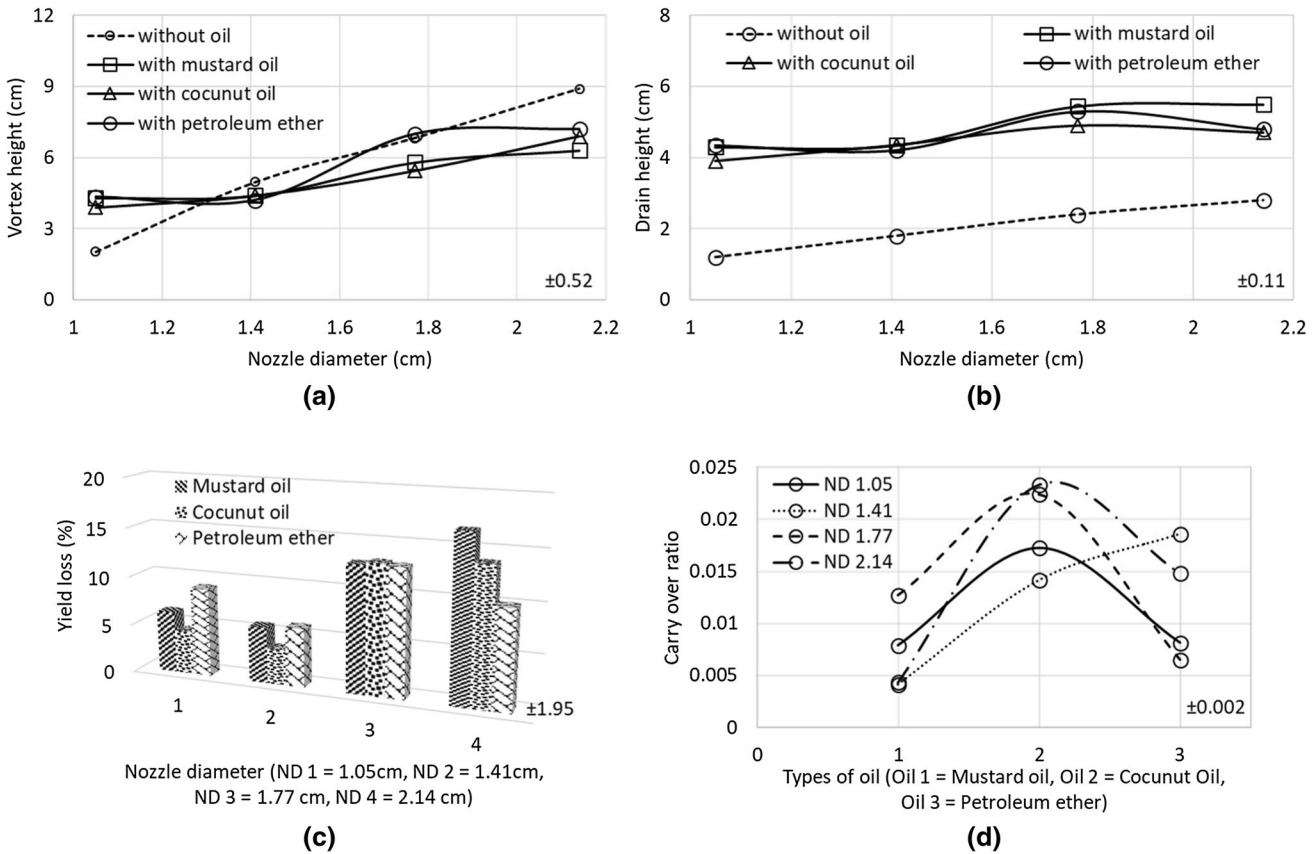


Fig. 9—Influence of overlying phase (oil) on (a) vortex height, (b) drain sink, (c) yield loss, and (d) COR. The numerical value on the right bottom corner of the figure represent the average standard deviation for all experimental data in the figure. Each experimental data represents the average value of two experimental trials.

liquid steel transfer operation. Some of the factors expected to change the vortex behavior in the BOF vessel in comparison to the ladle during the liquid steel transfer process are as follows.

1. The cross-sectional area of the BOF vessel varies with the LH; however, the ladle has an almost constant cross-sectional area during the transfer of liquid steel.
2. The nozzle is placed either at the center or eccentric position in the ladle. The increase in the eccentricity of the nozzle position decreases the critical height for vortex formation due to the extra time taken to align the vortex rotational axis to the exit nozzle axis.^[3,12] It is also observed that vortex formation is completely suppressed while placing the nozzle close to the ladle wall. However, in the BOF vessel, the nozzle is placed in the midplane shared by the cylinder and cone portion of the vessel.
3. The ferrostatic liquid head in the ladle will be higher than the BOF vessel; hence, the rate at which the LH decreases will be lesser in the BOF vessel than the ladle for the same quantity of liquid and constant ND.

4. The height-to-diameter ratio is different for the ladle and BOF vessel in the tapping position.

In this investigation, the combined effect of variable filling FR and DT is expected to provide the different magnitudes of residual motion in the liquid before the start of the tapping experiments.^[1,3] To simulate the increase in the tap hole diameter due to the erosion of refractories in plant practice, experiments were also performed with different NDs. An increase in ND increases the vortex height (refer to Figures 6(d) and 7(d)) as it accelerates the rotational velocity to a critical value sooner than the rate of discharge in the BOF vessel. This observation is in agreement with the findings of researchers^[14,15] for some of the conditions during the teeming process. However, the decrease in vortex height with the increase in initial filling FR and the decrease in DT for higher ND contradict the earlier reports.^[13–15] This difference in observation could be due primarily to the effect of a higher height-to-diameter ratio of the BOF vessel ($\frac{h}{d} = 4$) and the complex shape of the BOF vessel in comparison with the vessel having a constant cross-sectional-like

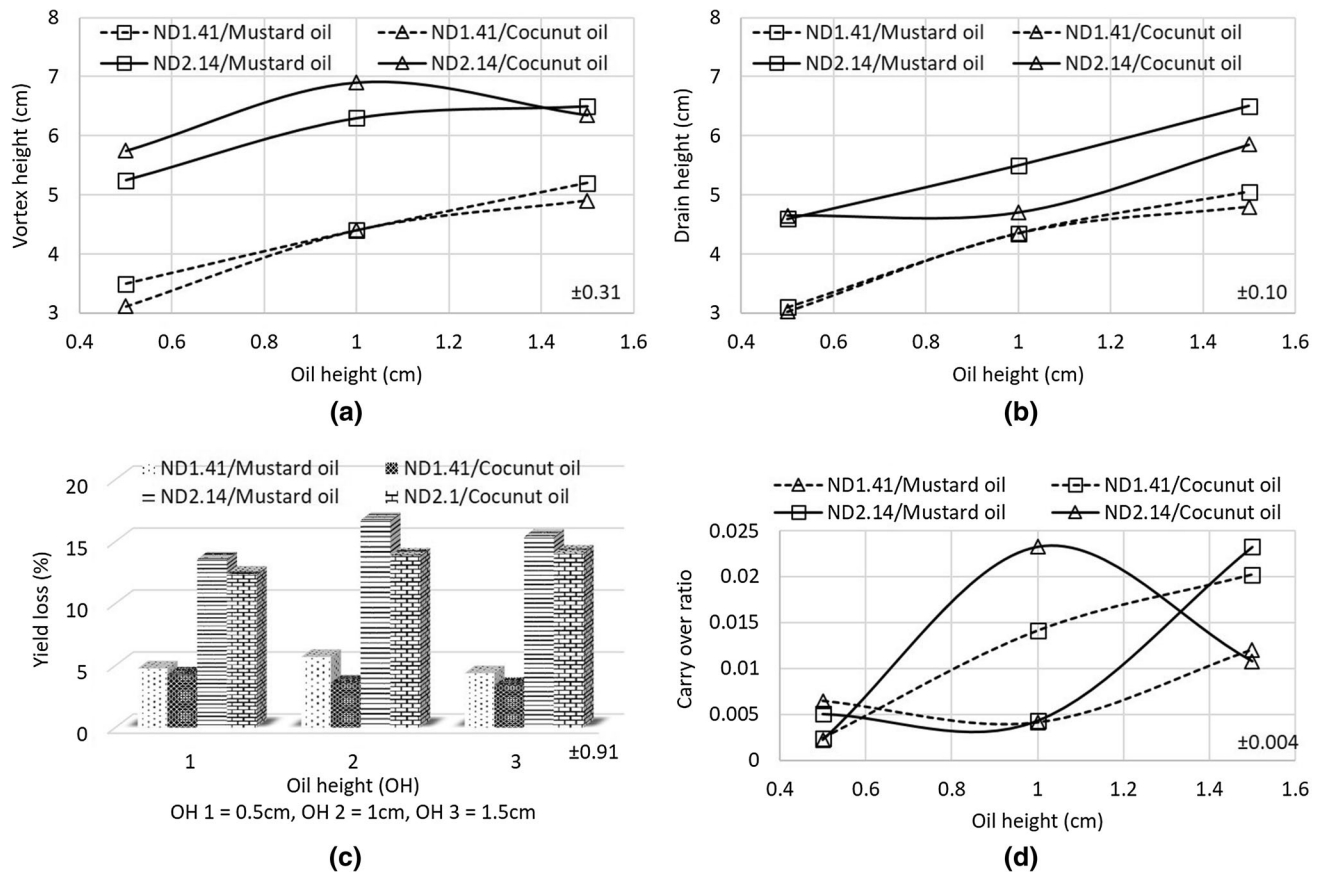


Fig. 10—Influence of amount of overlying phase (oil) on (a) vortex height, (b) drain sink, (c) yield loss, and (d) COR. The numerical value on the right bottom corner of the figure represent the average standard deviation for all experimental data in the figure. Each experimental data represents the average value of two experimental trials.

ladle ($\frac{h}{d} \leq 2$). In the case of the BOF vessel, the liquid also has to transfer from the rear end of the vessel to the tap hole zone in addition to the rotational velocity for vortex formation. Therefore, horizontal volume transfer (horizontal arrow in Figure 11) is also expected in addition to the vertical volume transfer (vertical arrow in Figure 11) in the vicinity of the tap hole. This horizontal movement of liquids from the rear end of the vessel is expected to prevent the full vortex establishment during tapping, as it generates fluid flow in the direction perpendicular to the discharge direction. The contradictory observation related to vortex formation in the present case (refer to Figures 6(a), (c) and 7(a), (c)) for higher FR and lower DT is attributed to the delay in angular momentum transfer (acceleration of rotational velocity) due to the combined effect of residual motion and horizontal volume transfer. Therefore, the present investigation clearly demonstrates the shape effect of the draining vessel on the occurrence of drain vortices during the liquid steel transfer process.

B. Dimensional Analysis

Many researchers^[3,8,10,12,14,15] developed correlations among various process parameters for predicting the onset of vortex events during the liquid steel draining processes. Investigators have also developed mathematical correlations for vortex formation in nonmetallurgical applications.^[37–41] However, almost all those studies were conducted using a vessel with the constant cross-sectional area, which differs from the design requirements for the BOF vessel. The observations in this study contrary to the available literature indicate that the occurrence of vortex formation during draining experiments in a rectangular or circular constant cross-sectional vessel would not simulate the actual condition during the BOF tapping process. Hence, an attempt has been made to develop new correlations among various parameters for estimation of vortex height, drain sink height, and yield loss during the BOF tapping process based on the dimensional analysis.

The critical height for vortex formation in the BOF vessel depends on the following parameters:

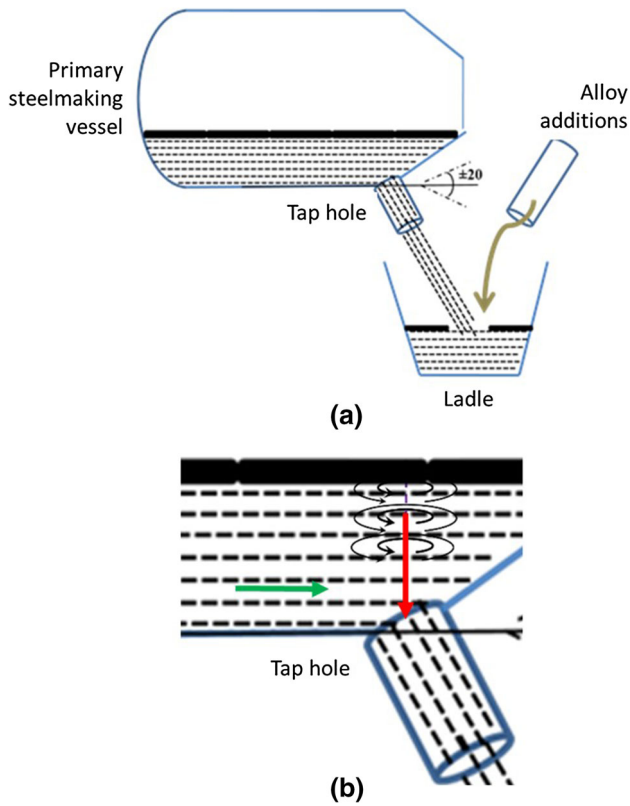


Fig. 11—(a) Sectional view of the tapping process and (b) representation of swirling motion, vertical, and horizontal volume transfer (indicated as an arrow) generated during the tapping process.

$$H_v = f(H_i, d, D, V, g, \mu, \rho, t), \quad [1]$$

where d is the nozzle/tap hole diameter; D is the characteristic length of the BOF vessel (length of liquid to travel from the rear end to the tap hole); H_i is the initial LH; V is the filling velocity (radius of the axial inlet filling pipe is 1.54 cm); g is the acceleration due to gravity; and μ and ρ are the dynamic viscosity and density of water at room temperature, respectively. Following the procedure of the Buckingham π theorem, various π numbers were identified.

$$\begin{aligned} \pi_1 &= \left(\frac{H_v}{H_i}\right), & \pi_2 &= \left(\frac{d}{H_i}\right) \\ \pi_3 &= \left(\frac{D}{H_i}\right), & \pi_4 &= \left(\frac{\rho V_0 H_i}{\mu}\right) \\ \pi_5 &= \left(\frac{gt^2}{H_i}\right), & \pi_6 &= \left(\frac{V^2}{gH_i}\right), \end{aligned}$$

where $V_0 = \sqrt{2gH_i}$ is the initial drain velocity as soon as the tap hole is opened. Among the preceding dimensionless groups, π_1 is the dimensionless dependent variable; $\left(\frac{\pi_2}{\pi_3}\right) = \left(\frac{d}{D}\right)$ is the geometrical scale down

parameter; π_4 is the Reynolds number (Re); π_5 is the nondimensional acceleration ratio governed by gravity, initial liquid head, and waiting time; and π_6 is the Froude number (Fr). The correlation for the prediction of the critical height for vortex formation is obtained as follows:

$$\left(\frac{H_v}{H_i}\right) = 4.4 \left(\frac{d}{D}\right)^{1.79} (\text{Fr})^{-0.05} \left(\frac{1}{\text{Re}}\right)^{0.63} \left(\frac{H_i}{gt^2}\right)^{-0.07} \times 10^5. \quad [2]$$

The coefficients are estimated by multivariable linear regression analysis based on the least-squares method^[42] using the experimental data.

The correlation for the prediction of the critical height for drain sink formation is estimated as follows:

$$\left(\frac{H_d}{H_i}\right) = 8.8 \left(\frac{d}{D}\right)^{1.21} (\text{Fr})^{-0.02} \left(\frac{1}{\text{Re}}\right)^{0.69} \left(\frac{H_i}{gt^2}\right)^{-0.001} \times 10^5. \quad [3]$$

To obtain the correlation for yield loss, the following parameters are considered:

$$W = f(w, d, H_i, Q, t, g) \quad [4]$$

where W is the weight of water remaining in the vessel after drain sink appears during the tapping process, w is the weight of water tapped into the collecting bath, Q is the initial filling FR (kg/s), and t is the waiting time. The following correlation is obtained for yield loss measurement:

$$\left(\frac{W}{w}\right) = 1.09 \left(\frac{H_i}{d}\right)^{1.70} \left(\frac{Q\sqrt{H_i}}{w\sqrt{g}}\right)^{-0.09} \left(\frac{H_i}{gt^2}\right)^{0.016}. \quad [5]$$

The variations of the estimated values of $\left(\frac{H_v}{H_i}\right)$, $\left(\frac{H_d}{H_i}\right)$, and $\left(\frac{W}{w}\right)$ using the dimensionless correlations in comparison with the results of the experiments are represented in Figures 12(a) through (c), respectively. All the figures clearly reveal that the estimated values corroborate well with the results of the water modeling experiments.

Similar correlations for vortex height and drain height have been obtained for water-oil experiments. The parameters considered for such correlations are given as follows:

$$H'_v(\text{or})H'_d = f(H_i, H_s, d, D, g, \Delta\mu, \Delta\rho, \Delta\sigma), \quad [6]$$

where H_s is the thickness of oil and $\Delta\mu$, $\Delta\sigma$, and $\Delta\rho$ are the difference in dynamic viscosity, surface tension, and density between water and oil, respectively. The initial filling FR and waiting time are maintained constant for all the water-oil experiments. The physical properties of the oils and water used in the calculation are given in Table II.^[43,44]

Correlation for estimation of the critical LH for vortex formation in the presence of the oil phase is derived as

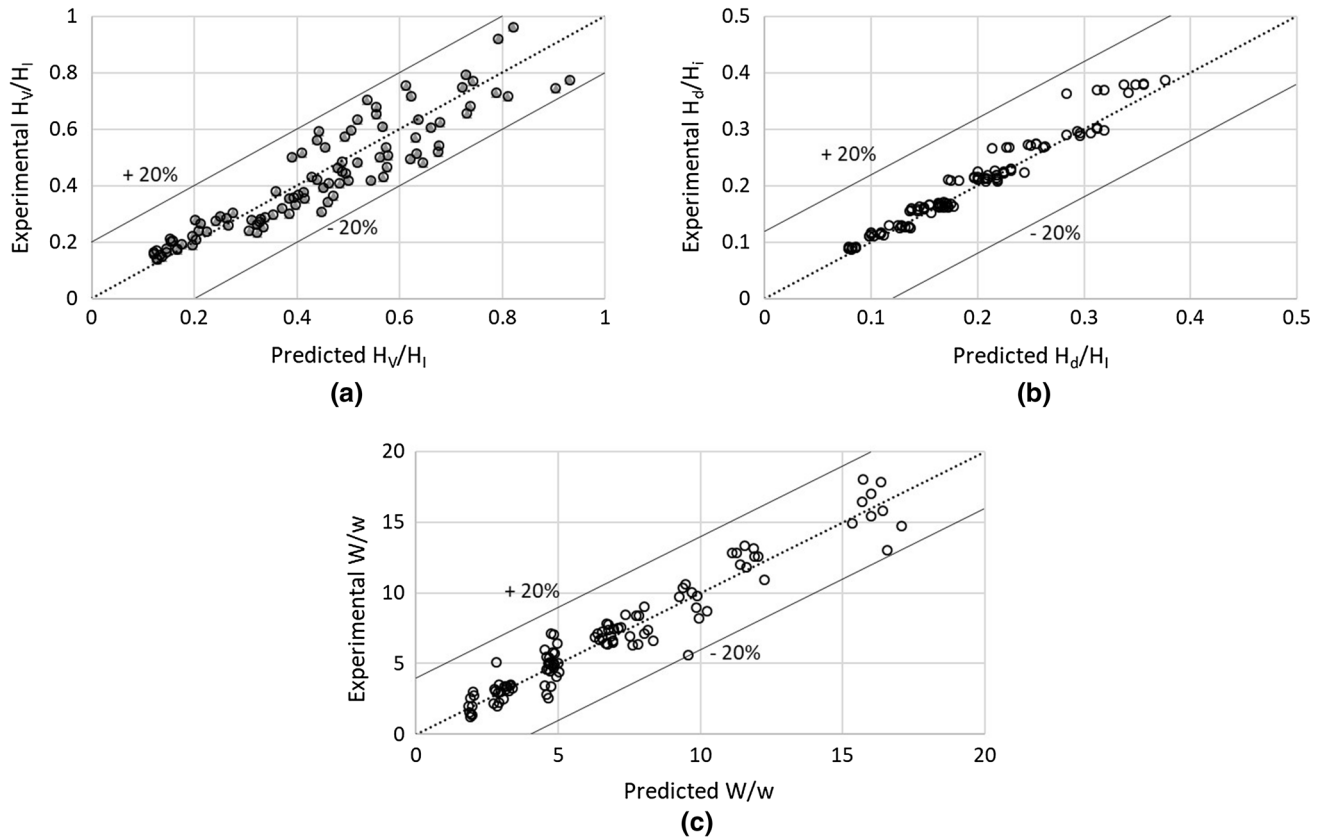


Fig. 12—Variation of predicted results with the experimental values: (a) vortex height, (b) drain height, and (c) yield loss for the experiments conducted without oil.

$$\left(\frac{H'_v}{H_s}\right) = 154 \left(\frac{d}{D}\right)^{0.77} \left(\frac{\Delta\sigma}{H_i^2 g \Delta\rho}\right)^{0.41} \left(\frac{\Delta\gamma}{H_i \sqrt{g H_i}}\right)^{-0.08} \quad [7]$$

Similarly, the critical LH for drain sink in the presence of the oil phase is derived as

$$\left(\frac{H'_d}{H_s}\right) = 36.5 \left(\frac{d}{D}\right)^{0.43} \left(\frac{\Delta\sigma}{H_i^2 g \Delta\rho}\right)^{0.34} \left(\frac{\Delta\gamma}{H_i \sqrt{g H_i}}\right)^{-0.04} \quad [8]$$

Here $\Delta\gamma$ is the difference in kinematic viscosity of water and oil. The variations of predicted values of $\left(\frac{H'_v}{H_s}\right)$ and $\left(\frac{H'_d}{H_s}\right)$ using the aforementioned dimensionless correlations with the results of water-oil experiments are represented in Figures 13(a) and (b). It is evident from the figure that the derived equations are in good agreement and capable of satisfactorily predicting the results of water modeling experiments. Therefore, the aforementioned correlations can be used for estimation of the critical height for the vortex and drain sink during the BOF tapping process in the presence of the overlying phase. Based on the reported^[12] hydrodynamic principles for ladle teeming, the formation of the vortex and drain sink during draining phenomena are generally not influenced by the physical properties of Newtonian fluid. Many researchers^[8,12-15] pointed

out that the initial condition (residual motion/tangential velocity) of liquid before the draining process from the teeming ladle has a major influence on vortex and drain sink formation. However, parameters, such as ND and initial LH, are independent of the initial condition of liquid and they have their own influence on vortex formation. This investigation has shed light on the influence of ND, initial LH, filling FR, and waiting time in the BOF vessel on vortex and drain sink formation using the BOF water model setup. The assumption of residual motion in the liquid controlled by the variable initial filling FR and DT (instead of supersonic jet, tilting, *etc.*) becomes the limitation of the present work.

C. Modified Empirical Correlation for Estimation of Slag Carryover in the Plant

An attempt was also made to predict the COR in the presence of the oil/slag phase in water modeling experiments. However, the successful estimation of the COR for water-oil experiments was not obtained due to the lesser number of such experiments. For estimation of the COR for plant data, a modified correlation was obtained using some relevant dimensionless numbers developed by Ashok *et al.*^[51] to predict the excess oxygen input into the ladle during tapping. The final empirical relationship is obtained as

Table II. Physical Properties of Water, Oil,^[43,44] Liquid Steel, and Slag^[54]

Solution Number	Liquid	Density (kg/m ³)	Viscosity (kg/ms)	Kinematic Viscosity (m ² /s)	Surface Tension at the Liquid-Liquid Interface (N/m)	Grade/Purity*
1	water	1000	0.0009125	9×10^{-7}	—	raw water
2	coconut oil	825	0.0229	3×10^{-5}	0.023	edible oil/99.9
3	mustard oil	875	0.07	8×10^{-5}	0.052	edible oil/99.75
4	petroleum ether	625	0.00038	6×10^{-7}	0.051	make rankem/99.97
5	liquid steel	7800	0.0077	9×10^{-7}	—	—
6	BOF slag**	2493 ± 0.5	0.25 ± 0.03	1×10^{-4}	$0.954 \pm 0.042^{**}$	—

*Purity: Based on volatile and insoluble contents (Fe, Cu, Pb, *etc.*).

**Average of the estimated values for the plant data studied.

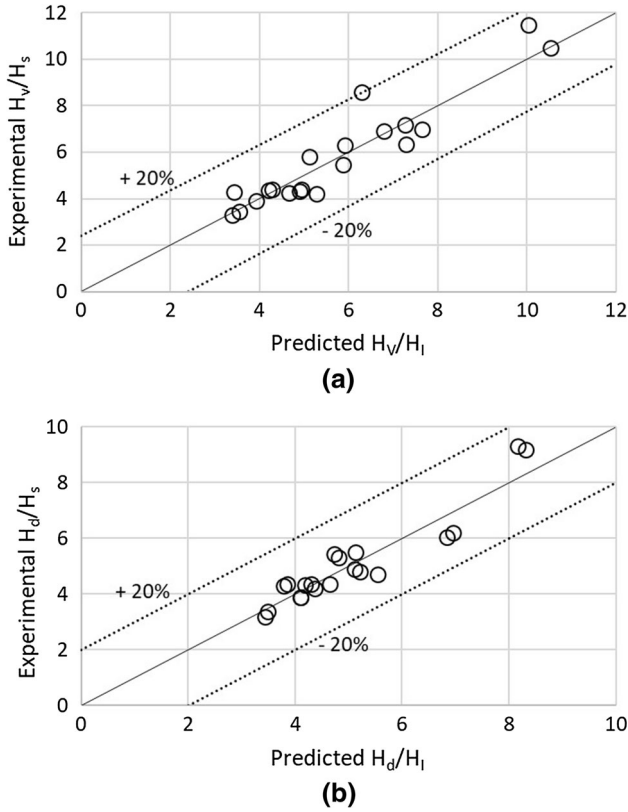


Fig. 13—Variation of predicted results with the experimental values: (a) vortex height and (b) drain height for the experiments conducted with oil.

$$\left(\frac{W_s}{w_m}\right) = -0.0179(T)^F + 105.82 \times 10^6 \left(\frac{\mu_s}{\sqrt{w_m \Delta \rho g}}\right) + 2405 \left(\frac{\sigma_{s-m}}{w_m^{2/3} g \Delta \rho^{1/3}}\right) + 0.0076(D)^F - 0.0064, \quad [9]$$

where $\left(\frac{W_s}{w_m}\right) = \text{COR}$, $W_s =$ weight of overlying phase (slag) carried over into the transfer ladle, $w_m =$ weight of underlying phase tapped during the tapping process, $(T)^F =$ temperature factor, and $(D)^F =$ deoxidation

factor. The COR for the plant data collected from an integrated steel plant was estimated by mass balance and using the equilibrium module in FactSage 6.4.^[54] It is known that the slag composition and temperature have a strong influence on both the kinematic viscosity and surface tension of the slag.^[45–47] The surface tension of liquid steel is also influenced by impurities such as carbon, sulfur, nitrogen, and oxygen.^[48–50] The slag-metal interfacial tension (σ_{s-m}) was calculated based on the method described by Mills^[52]:

$$\sigma_{s-m} = \sigma_m + \sigma_s - 2\varphi(\sigma_m \cdot \sigma_s)^{0.5}, \quad [10]$$

where σ_m and σ_s are the surface tension of the liquid steel and slag, respectively, and φ is an interaction coefficient. The surface tension of liquid steel at tapping temperature was calculated using the method proposed by Keisuke *et al.*:^[48]

$$\sigma_m = 1925 - 0.455(T - 1808) - 0.155T \ln \left(1 + 10^{-0.17W_o - 0.427W_c} W_o \exp\left(\frac{2.93 \times 10^4}{T} - 10.9\right) \right), \quad [11]$$

where W_C and W_O are the weight percent carbon and oxygen in the liquid steel, respectively. The surface tension of slag σ_s and the interaction coefficient φ for FeO-rich BOF slag were estimated using the following equations^[52]:

$$\sigma_s = \sum X_i \sigma_i = \sum X_1 \sigma_1 + X_2 \sigma_2 + X_3 \sigma_3 + \dots \quad [12]$$

$$\varphi = 0.5 + 0.3X_{\text{FeO}} \quad [13]$$

where X_i denotes the mole fraction of various slag constituents and σ_i is the surface tension of the pure components.^[52]

Kinematic viscosity of slag, $\gamma_s = \frac{\mu_s}{\rho_s}$, is estimated by calculating the μ_s using the viscosity module in FactSage and ρ_s by the method postulated by Milles.^[52] The physical properties of crude steel and BOF slag used in the calculation are also given in Table II. The estimated

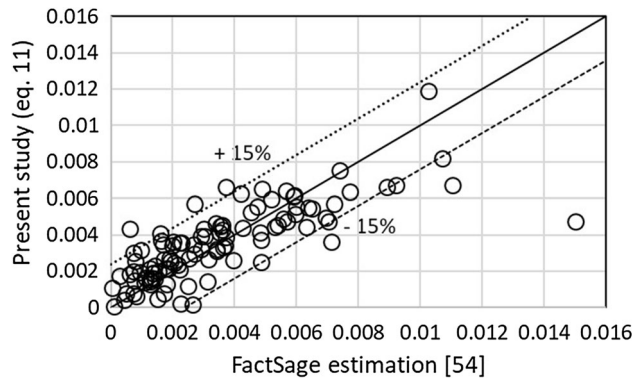


Fig. 14—Validation of COR predicted by the modified empirical equation with the FactSage estimated COR for the plant data.^[53]

physical properties of liquid steel and slag are in good agreement with the reported values.^[46–49] It is apparent from Figure 14 that the COR was predicted satisfactorily by the preceding equation for the plant data.

In the present study, different oils were studied to simulate the variation of physical properties of the slag at different tapping temperatures and slag compositions, especially the surface tension at the slag-liquid steel interface that varies noticeably. Table II tabulates the various physical properties of different oils and slags. The kinematic viscosities of mustard oil ($0.00008 \text{ m}^2/\text{s}$) and coconut oil ($0.00003 \text{ m}^2/\text{s}$) are comparable to that of the BOF slag ($0.0001 \text{ m}^2/\text{s}$), satisfying the dynamic similarity criterion for these oils to be used as low-temperature analogues for slag. The interfacial tension of steelmaking BOF slags varies in the range of 0.9 to 1.0 N/m.^[46–49] The low value of interfacial tension for the slag/liquid steel interface is attributed to the high value of ϕ (refer to Eq. [13]) due to the presence of higher FeO in the BOF slag. Petroleum ether and mustard oil used in the water modeling experiments possessed almost similar interfacial tension with water, which was higher than that of the coconut oil. Peranandhan and Mazumdar^[53] highlighted the influence of the interfacial tension on smaller scale phenomena, such as bubble size, shape, and free surface perturbations, in steelmaking operations. It is expected that the entrapment of the overlying phase during vortex formation will be enhanced with a decrease in interfacial tension, as observed in the case of coconut oil (refer to Figure 9(d)). It may be observed that slag viscosity is about one order of magnitude higher than the low-temperature analogue, which may be attributed to the presence of several solid phases in varying amounts in the liquid steel. The oils used in the present water-oil experiments also varied in viscosity to note the effect of viscosity on the vortex formation, and cold model experiments revealed no significant changes in the critical height for vortex formation (refer to Figures 9(a) and 10(a)) for different oils with varying viscosity. Contrary to our observation, the trend of decreasing critical height for vortex formation with an increase in the viscosity of oils was reported by Koria and Umakanth^[14] in the experiments conducted in a constant cross-sectional area tank (ladle). Therefore, the difference in vorticity dynamics in the

presence of the overlying phase during the BOF tapping process in comparison with the studies carried out in the constant cross-sectional area tank by the other researchers is also confirmed in this investigation. Equation [9], proposed for estimation of the COR in the plant, did not involve the design parameters and the process parameters that determine the initial liquid condition. It could be concluded that the onset of the vortex during the BOF tapping process could be principally controlled by vessel design and initial liquid conditions and that the COR is apparently influenced by the physicochemical aspects/properties of fluids and the process.

D. Mathematical Formulation of the Tapping Process

For the application of the present research work in the industry tapping process, an attempt is made to estimate the time for the critical height of vortex formation based on the macroscopic energy and mass balance approach. This will allow the operator to get an idea of the expected time for vortex formation so that necessary preventive action can be taken to control the slag carryover during the tapping process. The detailed derivation is given in the Appendix, and the instantaneous time for the various LHs in the BOF vessel during the tapping process can be represented as

$$t = \frac{4}{3C_d a_o \sqrt{2g}} \left[(2R - H)^{3/2} \left(D + \frac{2L}{15R} (4R + 3H) \right) \right]_{H_1}^{H_2}, \quad [14]$$

where R is the maximum height of liquid that can be filled in the BOF vessel in the tapping position, D is the distance from the rear end of the BOF vessel to the nozzle, H is the instantaneous LH in the LD vessel, C_d is the discharge coefficient, a_o is the cross-sectional area of the nozzle, and g is the acceleration due to gravity. The discharge coefficient C_d used in the calculation is 0.61, as the fabricated nozzles had sharp boundaries.^[55] The critical time for vortex (t_v) and drain sink (t_d) formation during tapping of water from the BOF vessel can be estimated by substituting H_2 as H_v and H_d , respectively. The estimated values of t_v and t_d corroborate well with the results of the water modeling experiments, as represented in Figures 15(a) and (b), respectively.

E. Industry Implication of the Present Study

In industrial steelmaking practice, slag carryover is generally controlled by employing IR imaging or slag cut-off devices (DART). As each of these technologies has its own limitation in arresting the carryover slag during tapping, a methodology to control the slag carryover without employing any external device is suggested by the present investigators based on the understanding developed using water modeling experiments.

Parametric analysis on vortex formation reveals that liquid movement generated perpendicularly to the descending direction of the LH in the BOF vessel resists or delays the vortex formation during the tapping

process. If the velocity of the liquid in the horizontal direction (V_h) is greater than the outflow velocity (V_{out}), it will break the vortex that exists vertically. It is important to note that the threshold velocity (V_h) requiring breaking of the existing vortex also decreases with time as $V_h > (V_{out} = \sqrt{2gH})$, where H denotes the instantaneous height of liquid steel. Figure 16 illustrates the application of this phenomenon to control slag carryover during the tapping process. During tapping experiments, it was observed that the vortex appeared right above the nozzle (perfect-vortex, shown in Figure 16(a)) or at off-center position (off-vortex, shown in Figure 16(b)) of the nozzle and extended toward the nozzle axis in the direction of outflow. In the present study, the critical time for vortex formation can be estimated using Eq. [14]. Once the critical time is known to the operator, tilt front or tilt back operation can be carried out to minimize the slag carryover. During this action, the axis of vortex rotation shifts from the nozzle exit axis and the vortex becomes unstable, as shown in Figures 16(c) and (d). It should be noted that application of tilt front or tilt back operation of the LD vessel generates bulk liquid motion in the direction perpendicular to the descending direction of the LH (indicated as wavy flow lines in Figures 16(c) and (d)). The vortex interaction volume in the liquid near the tap hole is small compared to the horizontal bulk liquid transfer from the rear end of the BOF vessel. Therefore, the stability of the vortex is disturbed by the horizontal bulk

flow. It results in delayed vortex formation, as observed for higher filling FR and lower DT (refer to Figure 6(c)) in the water model experiments. The similar observation is also reported by Kojola *et al.*[8] in an inclined and cone bottom ladle to enhance the yield during the liquid steel teeming process. Based on the preceding discussion, it can be stated that slag carryover during tapping can be minimized by controlling tilt back or tilt front operation without using any external devices, once the critical time for vortex formation is known.

It is important to note that some level of turbulence in the vessel is expected due to tilt front or tilt back operation, which may result in slag entrainment and wear of refractories away from the vortex region. However, it is also expected that the cosplashing or coating of the BOF slag on the furnace wall due to the turbulence generated during induced tilting will protect the furnace refractories. To break the vortex toward the end of the tapping process, a minimal amount of tilting may be sufficient to generate induced flow in the horizontal direction. This is mainly due to the smaller threshold horizontal velocity (to break the vortex) required with the decrease in the LH during tapping, as discussed earlier. Further investigation in this direction is required to optimize the extent of the induced tilting operation for the tapping process.

V. CONCLUSIONS

In the present investigation, the BOF tapping process is simulated using a geometrical down-scaled Perspex semi-BOF cold model. This investigation brought out the influence of complex BOF shape on drain vortices during liquid steel tapping from the BOF vessel in comparison with the ladle teeming operations. The salient points that emerged out of the present investigation are as follows.

1. Drain curve analysis reveals that the initial water filling FR and DT of liquid steel in the vessel before tapping have negligible influence on the drain curves.
2. The tap hole diameter strongly influences the critical LH for vortex and drain sink formation as well as yield loss during tapping. The FR and DT also influence the vortex height only when the ND is higher.
3. The presence of the overlying phase decreases the critical height for vortex (except ND 1.05 cm) formation. However, it increases the critical height for drain sink formation. Vortex height, drain sink height, and yield loss increase with the increase in the amount of overlying phase. Yield loss during the tapping process increases with the increase in tap hole diameter with and without the overlying phase.
4. The correlations for prediction of critical heights for vortex and drain sink formation during the tapping process were successfully established based on the dimensional analysis by considering the presence and absence of the overlying phase.
5. Dimensionless correlation for the slag COR (defined as the ratio of the amount of slag carryover to the

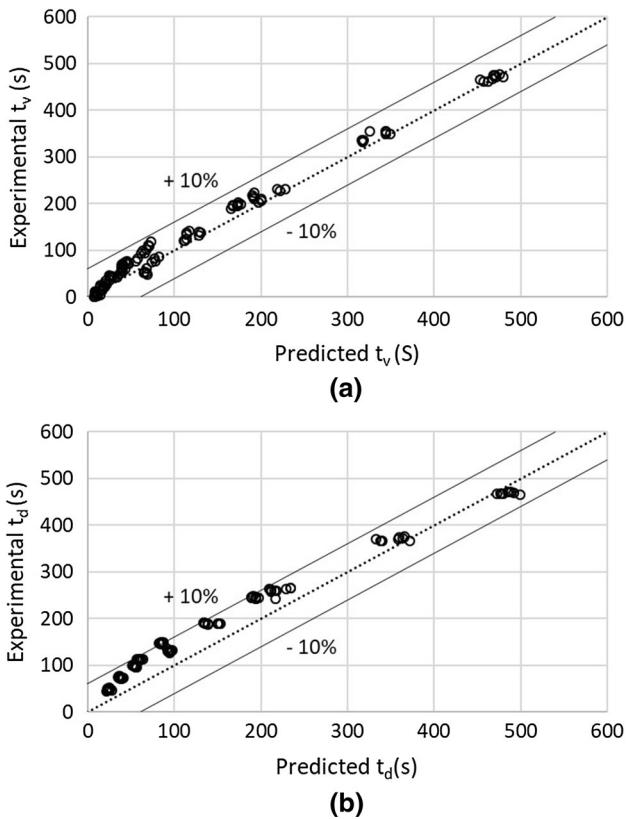


Fig. 15—Variation of predicted results with the experimental values: (a) vortex time and (b) drain sink time for the experiments conducted without oil.

amount of liquid steel tapped during tapping) has also been developed for application to industrial data. The predicted COR is found to be in agreement with the estimated slag COR for industrial practice, which has been obtained based on the mass balance approach using FactSage simulation for the plant data. It is concluded that the onset of vortex during the tapping process is primarily influenced by the vessel design; however, the amount of slag carryover is influenced by the physicochemical properties of slag.

6. Based on the study, it is inferred that slag carryover during the tapping process can be minimized by controlling tilt back or tilt front operation without using any external devices, once the critical time for vortex formation is known.

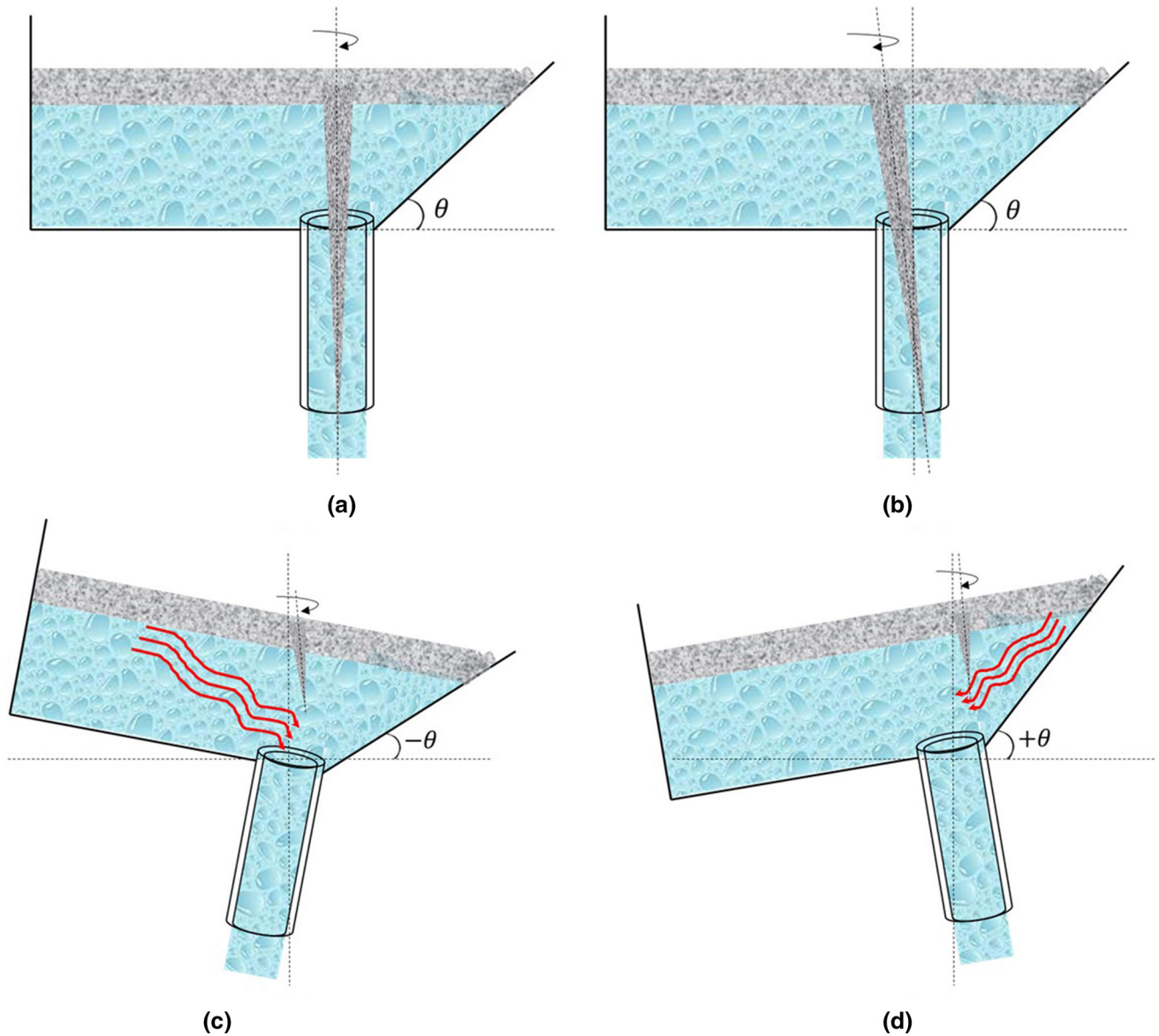
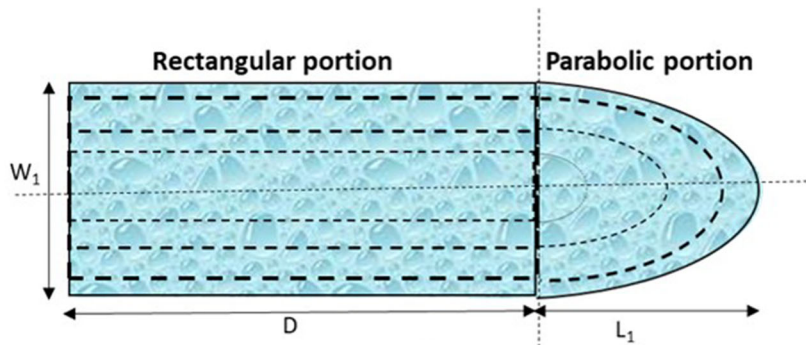


Fig. 16—Strategy to control slag carryover during the industrial tapping process: (a) perfect vortex and (b) off-vortex, vortex breaking by (c) tilt front and (d) tilt back operation.

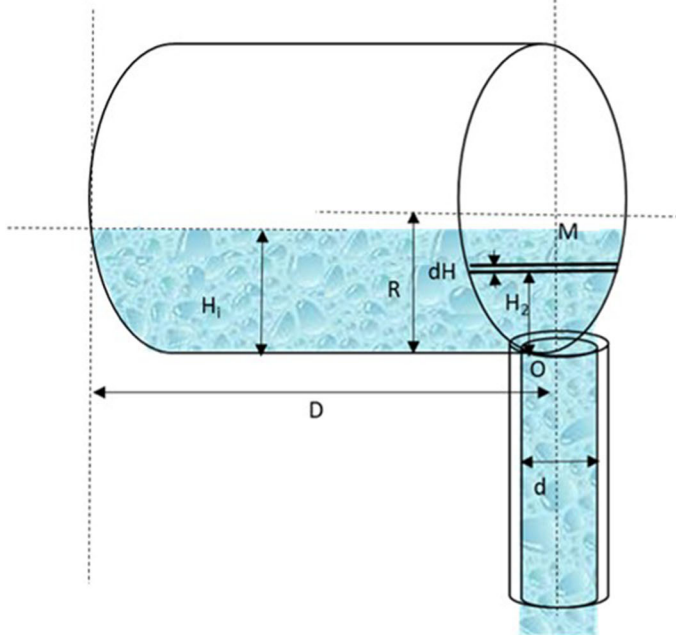
Fig. A1—Detailing of the BOF tapping process for mathematical formulation: (a) variable cross section from the top view (indicated as dashed lines of difference thickness), (b) detailing along the cylinder-cone joining plane to solve for the variable cross-sectional area of the cylinder portion, and (c) detailing along the plane MNO to solve for the variable cross-sectional area of the cone portion.

APPENDIX

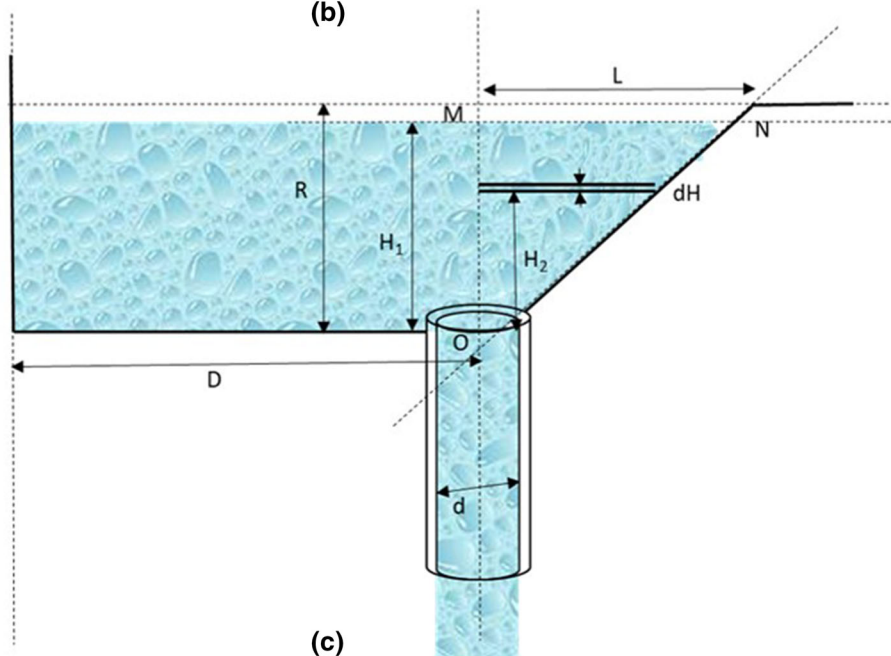
The BOF vessel in the tapping position is divided into two parts: (1) a horizontal cylindrical portion and (2) a conical portion. A tap hole is located in the midplane joining the horizontal cylinder and the cone of the vessel. It should be noted that the cross-sectional area of



(a)



(b)



(c)

the BOF vessel in the tapping position (A) will decrease with a decrease in LH, as indicated by the dashed lines in the variable thickness in Figure A1(a). Therefore, the total cross-sectional area (A) of the BOF vessel in the tapping position can be calculated by the addition of the cross-sectional area of the cylinder (A_{cy}) and cone (A_{co}):

$$A = A_{cy} + A_{co} \quad [A1]$$

Solving for the plane that connects the cylinder and cone represented in Figure A1(b), the cross-sectional area of the tank in the cylinder portion can be derived as

$$A_{cy} = 2D\sqrt{2RH - H^2} \quad [A2]$$

where R is the maximum height of liquid that can be filled in the LD vessel in the tapping position, D is the distance from the rear end of the LD vessel to the nozzle, and H is the instantaneous LH in the LD vessel.

The cross-sectional area of the cone portion of BOF vessel in the tapping position is a parabola, as shown in Figure A1(a). The area of a paraboloid for the cone portion can be represented as

$$A_{co} = \frac{2}{3} W_1 L_1, \quad [A3]$$

where W_1 and L_1 are vessel dimensions, as represented in Figure A1(a). Solving for the triangular plane MNO, as shown in Figure A1(c), which intersects the midplane perpendicularly, the area of the paraboloid can be rewritten as

$$A_{co} = \frac{2}{3} W_1 L_1 = \frac{4}{3} \left(2\sqrt{2RH - H^2} \right) \frac{HL}{R}. \quad [A4]$$

The rate of change of liquid volume in BOF vessel equals the rate of outflow through the tap hole. Therefore, the volumetric FR (q) through the tap hole can be represented as

$$q = C_d a_o \sqrt{2gH} = -A \frac{dH}{dt} \quad [A5]$$

$$\int_0^t dt = \frac{-1}{C_d a_o \sqrt{2g}} \int_{H_1}^{H_2} \frac{A}{\sqrt{H}} dH, \quad [A6]$$

where C_d is the discharge coefficient, a_o is the cross-sectional area of the nozzle, and g is the acceleration due to gravity. Substituting $A = A_{cy} + A_{co}$ in Eq. [A6],

$$\int_0^t dt = \frac{-1}{C_d a_o \sqrt{2g}} \int_{H_1}^{H_2} \frac{\left(2D\sqrt{2RH - H^2} + \frac{4}{3} \left(2\sqrt{2RH - H^2} \right) \frac{HL}{R} \right)}{\sqrt{H}} dH. \quad [A7]$$

After deducing, instantaneous time (t) for various LHs can be represented as

$$t = \frac{4}{3C_d a_o \sqrt{2g}} \left[(2R - H)^{3/2} \left(D + \frac{2L}{15R} (4R + 3H) \right) \right]_{H_1}^{H_2}. \quad [A8]$$

The BOF vessel constants, D , L and R , used in Eq. [A8] are shown in Figure A1.

NOMENCLATURE

H_i (LH)	Initial liquid height (m)
d (ND)	Nozzle/tap hole diameter (m)
Q (FR)	Initial water filling flow rate (lpm/kg s ⁻¹)
t (DT)	Dwell/waiting time (s)
COR	Carryover ratio (—)
H_v	Critical LH for vortex formation (m)
H_d	Critical LH for drain sink formation (m)
w_m	Weight of water/liquid steel tapped during tapping (kg)
W_s	Weight of oil/slag carried over during tapping (kg)
D	Distance from rear end of LD vessel to the tap hole (m)
V	Initial water filling velocity (m s ⁻¹)
H	Instantaneous LH in LD vessel during tapping (m)
g	Acceleration due to gravity (m ² s ⁻¹)
ρ	Density (kg m ⁻³)
μ	Dynamic viscosity (kg m ⁻¹ s ⁻¹)
σ	Surface tension (N m ⁻¹)
γ	Kinematic viscosity (m ² s ⁻¹)
σ_{s-m}	Interfacial tension of liquid steel and slag (N m ⁻¹)
C_d	Discharge coefficient (—)
a_o	Cross-sectional area of tap hole/nozzle (m ²)
Fr	Froude number (—)
Re	Reynolds number (—)

REFERENCES

1. L.M. Trefethen, R.W. Bilger, P.T. Fink, R.E. Luxton, and R.I. Tanner: *Nature*, 1965, vol. 207, pp. 1084–85.
2. B.T. Lubin and G.S. Springer: *J. Fluid Mech.*, 1967, vol. 29 (Part 2), pp. 385–90.
3. R. Sankaranarayanan and R.I.L. Guthrie: *Ironmak. Steelmak.*, 2002, vol. 29, pp. 147–53.
4. G.S. Oiaz, A.R. Banderas, J. de J. Barreto, and R.O. Morales: *Steel Res. Int.*, 2007, vol. 78, pp. 248–53.
5. A. Muralikrishna, S. Bagui, and D. Mazumdar: *Trans. Ind. Inst. Met.*, 2013, vol. 66, pp. 281–95.
6. D. Mazumdar, O.P. Singh, J. Dutta, S. Ghosh, D. Satish, and S. Chakraborty: *Trans. Ind. Inst. Met.*, 2011, vol. 64, pp. 593–605.
7. K. Michalek, K. Gryc, L. Socha, M. Tkadlečková, M. Saternus, J. Pieprzyca, T. Merder, and L. Pindor: *Arch. Metall. Mater.*, 2016, vol. 61, pp. 257–60.
8. N. Kojola, S. Takagi, S. Yokoya, and P. Jönsson: *ISIJ Int.*, 2009, vol. 49, pp. 1–9.
9. S.H. Majidi and C. Beckermann: Paper presented at *Proc. 70th SFSA Technical and Operating Conference*, Steel Founders' Society of America, Chicago, IL, 2016, paper no. 4.8.
10. P.K. Singh: Master's Thesis, University of Kentucky, Lexington, KY, 2004.

11. G. Caruso, L. Cristofano, M. Nobili, and D. Vitale Di Maio: *J. Phys. Conf. Ser.*, 2014, vol. 501, pp. 1–10.
12. H.X. Li, Q. Wang, J.W. Jiang, H. Lei, Z.C. Guo, and J.C. He: *ISIJ Int.*, 2016, vol. 56, pp. 94–102.
13. P. Hammerschmid, K.H. Tacke, H. Popper, L. Weber, M. Dubke, and K. Schwerdtfeger: *Ironmak. Steelmak.*, 1984, vol. 11, pp. 332–39.
14. S.C. Koria and P. Umakanth: *Steel Res.*, 1994, vol. 65, pp. 8–14.
15. S.C. Koria and P. Umakanth: *Trans. Ind. Inst. Met.*, 1994, vol. 47, pp. 121–30.
16. O. Davila, R.D. Morales, and L.G. Demedices: *Metall. Mater. Trans. B*, 2006, vol. 37B, pp. 71–87.
17. G.M. Mazzaferro, M. Piva, S.P. Ferro, P. Bissio, M. Iglesias, A. Calvo, and M.B. Goldschmit: *Ironmak. Steelmak.*, 2004, vol. 31, pp. 1–6.
18. K. Kuwana, M.I. Hassan, P.K. Singh, K. Saito, and J. Nakagawa: *Mater. Manuf. Process.*, 2008, vol. 23, pp. 407–12.
19. R.D. Morales, O.D. Maldonado, I. Calderón, and K.M. Higa: *ISIJ Int.*, 2013, vol. 53, pp. 782–91.
20. M.B. Goldschmit, S.P. Ferro, and A.H.C. Owen: *Progr. Compu. Fluid Dyn. Int. J.*, 2004, vol. 4, pp. 12–19.
21. G.J. Hassall: Report No. 7210-CB/805, British Steel Corporation, European Commission, London, 1948.
22. H. Doostmohammadi, M. Andersson, K. Stenholm, and P. Jonsson: *Effect of EAF Slag Carryover on Slag-Metal Equilibrium Calculations for Ladle Degassing Process. TMS Annual Meeting and Exhibition*, TMS, San Francisco, 2009.
23. C.J.Z. Yiyu and Z. Lixin: Progress of Production Technology of Clean Steel in Bao Steel. http://www.baosteel.com/english_n/e07tchnical_n/021402e.pdf. Accessed 28 July 2018.
24. E.K. Mattias: *Know the Unknown: How Carry-Over Slag Varies and How It Impacts on the Processing and Product Quality in Metals Production*, Metsol AB, Stockholm, 2013.
25. R.J. Fruehan and S. Misra: “Hydrogen and Nitrogen Control in Ladle and Casting Operations,” AISI/DOE Technology Roadmap Program Report, Carnegie Mellon University, Pittsburgh, PA, 2005.
26. Z. Adolf, I. Husar, and P. Suchánek: *Mater. Technol.*, 2007, vol. 41, pp. 185–88.
27. K. Stenholm, N.A.I. Andersson, A. Tilliander, and P.G. Jönsson: *Ironmak. Steelmak.*, 2016, vol. 45, pp. 114–24.
28. J. Alexis, M. Andersson, J. Björkvall, D. Sichen, and A. Sandberg: Report No. JK 23045, Strategic Steel Research Programme for Sweden 2007–2012, jointly funded by VINNOVA and Jernkontoret, Sweden, 2011.
29. J.L. Liow, M. Juusela, and N.B. Gray: “Viscosity Effects in the Discharge of a Two-Layer Liquid through an Orifice,” *14th Austr. Fluid Mechanics Conf.*, Adelaide, Australia, Dec. 10–14, 2001, pp. 853–56.
30. J.W. Suh, J. Park, H. Kim, and Z.H. Lee: *ISIJ Int.*, 2001, vol. 41 (7), pp. 689–95.
31. E.K. Mattias: *Advanced Vision Systems to Control Ladle Slag Carry-Over*, METEC & 2nd ESTAD, Düsseldorf, June 15–19, 2015.
32. E.A. Fuchs, D.A. Goldstein, and A. Sharan: Patent No. EP 0922774 A1, Bethlehem Steel Corporation, Bethlehem, PA, 1998.
33. J.A. Stofanak, A. Sharan, D.A. Goldstein, and E.A. Stelts: Patent No. US 6197086 B1, Bethlehem Steel Corporation, Bethlehem, PA, 2001.
34. W. Purchase: Patent No. US 6602069 B2, Goricon Metallurgical Services Limited, 2003.
35. F. Rubenzuckera, R. Krumpa, M. Borza, K. Hölzla, and M. Traugott: Improvements for LD-Converter & Electric Arc Furnaces, METAL (2005). <http://konference.tanger.cz/data/metal2005/sbornik/papers/219.pdf>. Accessed 28 July 2018.
36. S.J. Lee, S.J. Kim, and H.G. Lee: *Met. Mater. Int.*, 2016, vol. 22 (1), pp. 136–42.
37. F.M. Sakri, M.S.M. Ali, S. Ahmad, Z.S. Salim, and S. Muhamad: *IOP Conf. Ser.: Mater. Sci. Eng.*, 2017, vol. 226, pp. 1–11.
38. D. Agarwal, P. Basu, T.J. Tharakan, and A. Salih: *Aerosp. Sci. Technol.*, 2017, vol. 32, pp. 60–65.
39. C.H. Sohn, M.G. Ju, and B.H.L. Gowda: *J. Mech. Sci. Technol.*, 2010, vol. 24, pp. 951–60.
40. J. Mohammadi, H. Karimi, M. Islami, and M.H. Hamed: *Adv. Mech. Eng.*, 2012, pp. 1–5.
41. A. Tinaikar, S. Advait, and S. Basu: *J. Fluid Mech.*, 2018, vol. 836, pp. 873–909.
42. M. Douglas: *Design of Analysis and Experiments*, 8th ed., Wiley Publisher, North California, 2013, pp. 449–77.
43. N. Siddiqui and A. Ahmad: *Int. J. Sci. Environ. Technol.*, 2013, vol. 2, pp. 1318–26.
44. Database Oil Properties, Environment Technology Center, Canada. http://www.etc-cte.ec.gc.ca/databases/Oilproperties/pdf/WEB_Petroleum_Ether.pdf, 2001. Accessed 28 July 2018.
45. A. Jakobsson, M. Nasu, J. Mangwiru, K.C. Mills, and S. Seetharaman: *Philos. Trans. R. Soc. Lond. A*, 1998, vol. 356, pp. 995–1001.
46. H. Sun, K. Nakashima, and K. Mori: *ISIJ Int.*, 2006, vol. 46, pp. 407–12.
47. E.J. Jung, W. Kim, I. Sohn, and D.J. Min: *J. Mater. Sci.*, 2010, vol. 45, pp. 2023–29.
48. K. Morohoshi, M. Uchikoshi, M. Isshiki, and H. Fukuyama: *ISIJ Int.*, 2013, vol. 53, pp. 1315–19.
49. K. Ogino, S. Hara, Takashi, and S. Kimoto: *ISIJ Int.*, 1984, vol. 24, pp. 522–31.
50. R.F. Brooks and P.N. Quedsted: *J Mater. Sci.*, vol. 40, pp. 2233–38.
51. K. Ashok, G.G. Roy, and G.K. Mandal: *Trans. Ind. Inst. Met.*, 2017, vol. 17, pp. 2465–76.
52. K.C. Mills: “The Estimation of Slag Properties,” Southern African Pyrometallurgy, unpublished research, 2011.
53. M. Peranandhanthan and D. Mazumdar: *ISIJ Int.*, 2010, vol. 50, pp. 162–231.
54. K. Ashok, G.G. Roy, and G.K. Mandal: *Modeling and Simulation Studies on BOF Tapping Process, 3rd Internation Conference of Ironmaking and Steelmaking*, Kanpur, 2017, pp. 403–06.
55. C. Schaschke: *Fluid Mechanics*, Institution of Chemical Engineers, Rugby, UK, 2000, p. 141.